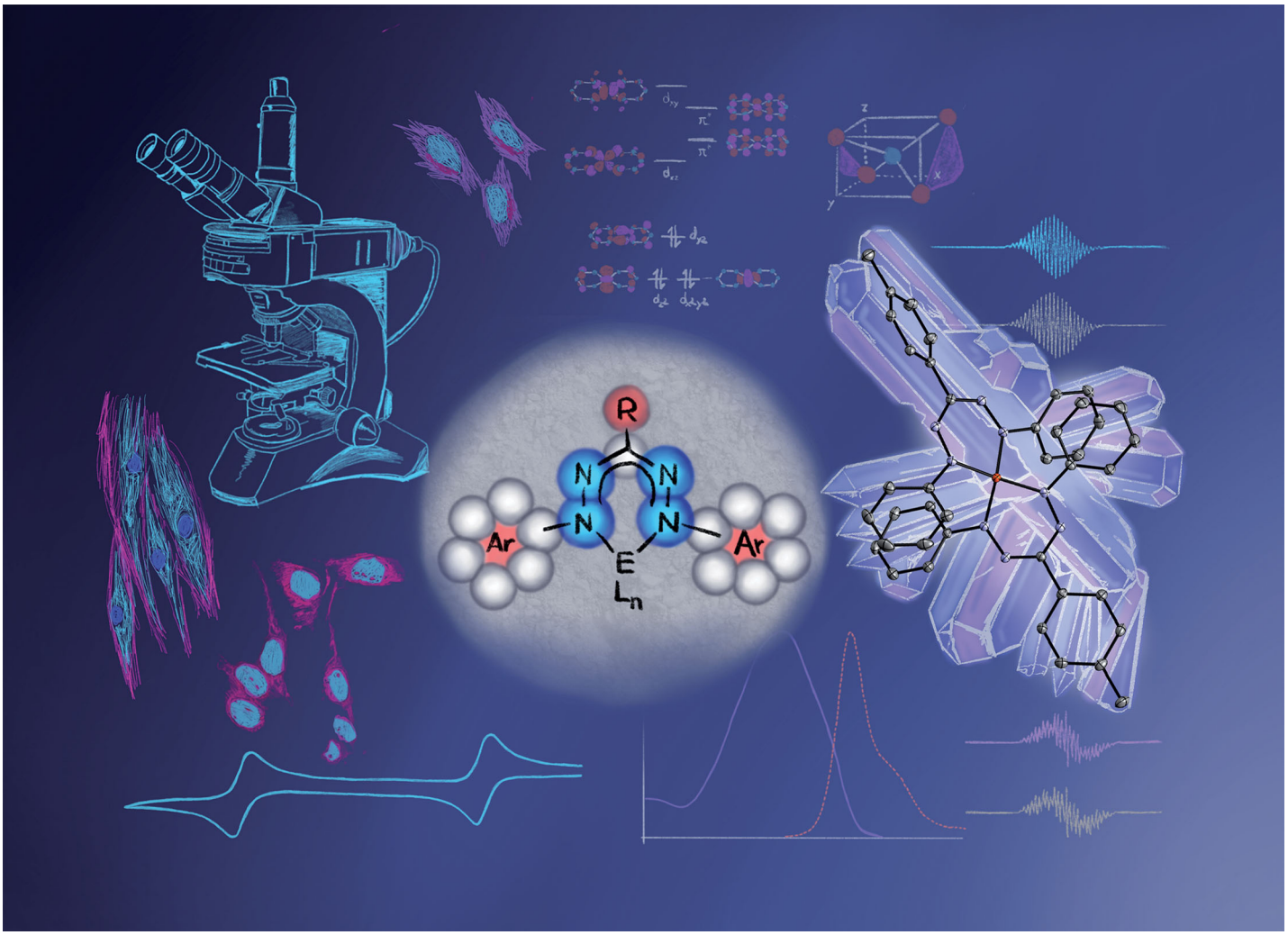

Showcasing research from the research groups of Professor Gilroy, Department of Chemistry, The University of Western Ontario, Canada, and Professor Otten, Stratingh Institute for Chemistry, University of Groningen, The Netherlands. The cover artwork was prepared by Jana Volarić.

Formazanate coordination compounds: synthesis, reactivity, and applications

The structural and (opto)electronic features of formazanate ligands provide their coordination compounds with novel properties for applications ranging from catalysis to imaging.

As featured in:

See Joe B. Gilroy and Edwin Otten, *Chem. Soc. Rev.*, 2020, **49**, 85.

ROYAL SOCIETY OF CHEMISTRY

rsc.li/chem-soc-rev

Registered charity number: 207890

Chem Soc Rev

REVIEW ARTICLE

View Article Online
View Journal | View Issue

Cite this: *Chem. Soc. Rev.*, 2020, **49**, 85

Formazanate coordination compounds: synthesis, reactivity, and applications

Joe B. Gilroy *[a] and Edwin Otten *[b]

Formazans (Ar[1]-NH-N=CR[3]-N=N-Ar[5]), a class of nitrogen-rich and highly colored compounds, have been known since the late 1800s and studied more closely since the early 1940s. Their intense color has led to their widespread use as dyes, especially in cell biology where they are most often used to quantitatively assess cell-viability. Despite structural similarities to well-known ligand classes such as β-diketiminates, the deprotonated form of formazans, formazanates, have received relatively little attention in the transition metal and main group coordination chemistry arenas. Formazanate ligands benefit from tunable properties *via* structural variation, rich optoelectronic properties owing to their highly delocalized π-systems, low-lying frontier orbitals that stabilize otherwise highly reactive species such as radicals, and redox activity and coordinative flexibility that may have significant implications in their future use in catalysis. Here, we review progress in the coordination chemistry of formazanate ligands over the past two decades, with emphasis on the reactivity and applications of the subsequent complexes.

Received 27th September 2019

DOI: 10.1039/c9cs00676a

rsc.li/chem-soc-rev

[a] *Department of Chemistry and The Centre for Advanced Materials and Biomaterials Research (CAMBR), The University of Western Ontario, London, ON, Canada N6A 5B7. E-mail: joe.gilroy@uwo.ca*

[b] *Stratingh Institute for Chemistry, University of Groningen, Nijenborgh 4, 9747 AG Groningen, The Netherlands. E-mail: edwin.otten@rug.nl*

1. Introduction

Formazans **1** were first reported in the 1890s, although they have only been studied extensively since the early 1940s.[1–3] The intense color and redox-chemistry that originates from

Joe B. Gilroy

Joe Gilroy is an Associate Professor in the Department of Chemistry at The University of Western Ontario (aka Western University). Originally from the West Coast of Canada, he completed both his BSc and PhD at the University of Victoria where he conducted research in stable radical chemistry under the supervision of Prof. Robin Hicks. He moved to the University of Bristol for his postdoctoral studies where he worked in various areas of metallo-polymer chemistry with Prof. Ian Manners as an NSERC and EU Marie Curie PDF. At Western, Joe leads a talented team of students and postdocs who work in many different areas of synthetic materials chemistry, with major focuses including the development of luminescent and semiconducting molecular and polymeric materials. He has received several awards, including the Thieme Chemistry Journal Award, Western's Petro-Canada Young Innovator and Faculty Scholar Awards, the CNC-IUPAC travel award, and an Ontario Early Researcher Award.

Edwin Otten

Edwin Otten is an Associate Professor in the Stratingh Institute for Chemistry at the University of Groningen. He obtained a PhD in chemistry in 2008 (supervisor: Prof. Bart Hessen, University of Groningen). He subsequently moved to the University of Toronto as a NWO Rubicon postdoctoral fellow, where he worked on small-molecule activation by Frustrated Lewis Pairs with Prof. Doug Stephan. After a short period in industry (SABIC), Edwin was appointed as tenure-track Assistant Professor of Molecular Inorganic Chemistry at the University of Groningen in 2011. In the same year he was awarded a Veni grant, and in 2015 he received a Vidi grant from NWO. His research focuses on the development of new (catalytic) reactions using metal complexes with ligands that incorporate reactive ('non-innocent') sites. In addition, he is interested in ligand design for manipulating the electronic structure of main group and transition metal complexes, and how this impacts reactivity.

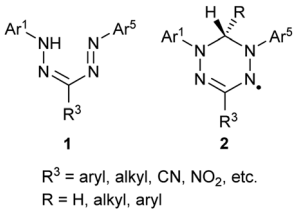

Chart 1

their nitrogen-rich backbone has led to their widespread use as dyes, mainly in chemical biology as the colored component of cell-viability assays,[4,5] and as precursors to a family of stable radicals known as verdazyls **2** (Chart 1).[6–8]

The Ar^1-NH-N=CR^3-N=N-Ar^5 backbone of formazans provides a platform for structural isomerization (Fig. 1). Bulky alkyl or aryl R^3 substituents tend to favor the 'closed' (*trans–syn*, s-*cis*) isomer, while relatively small R^3 substituents (*e.g.*, H, Me, SMe, CN) allow for the 'open' (*trans–syn*, s-*trans*) and 'linear' (*trans–anti*, s-*trans*) geometry to be adopted. There is a strong correlation between the identity of the isomer adopted and the color of formazans, with the 'closed' isomer exhibiting a characteristic blood red color, while the 'open' and 'linear' forms taking on orange and yellow colors, respectively.

One of the most intriguing features of formazan chemistry is their facile synthesis that allows for libraries of compounds to be prepared and facilitates property modulation through structural variation. While numerous synthetic routes to formazans exist,[1] the most widely employed methods rely on the reaction of aryldiazonium salts with substrates possessing activated carbon functionalities. For example, triarylformazans **3** can be prepared by coupling one equivalent of aryl diazonium salt with hydrazones (Scheme 1a).[1,9] This method is modular and provides access to asymmetric formazans with different Ar^1 and Ar^5 substituents, and can also be employed to prepare 3-alkyl formazans **4** (Scheme 1b).[1,10–12] Alternatively, coupling two equiv. of aryldiazonium salts with compounds containing activated methylene groups yields symmetric formazans ($Ar^1 = Ar^5$). Thus, two equiv. of aryldiazonium salts react with the activated methylene group of phenylpyruvic acid derivatives to give triarylformazans **3** (Scheme 1c).[1,13] Similar reactions lead to the formation of 3-cyanoformazans **5** (Scheme 1d)[1,14] and 3-nitroformazans **6** (Scheme 1e).[14,15] Although the yield of formazan products using these procedures is often moderate to good (typically 40–80%), the stability of the requisite diazonium salts may present problems, in particular when sterically demanding substituents are introduced.

Despite their structural similarity to other families of chelating N-donor ligands (*e.g.*, β-diketiminates **7**),[16,17] it may

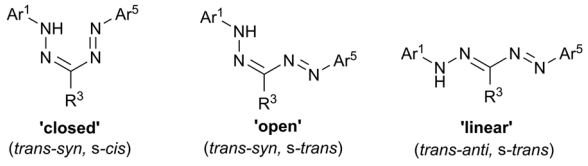

Fig. 1 Structural isomers of formazans.

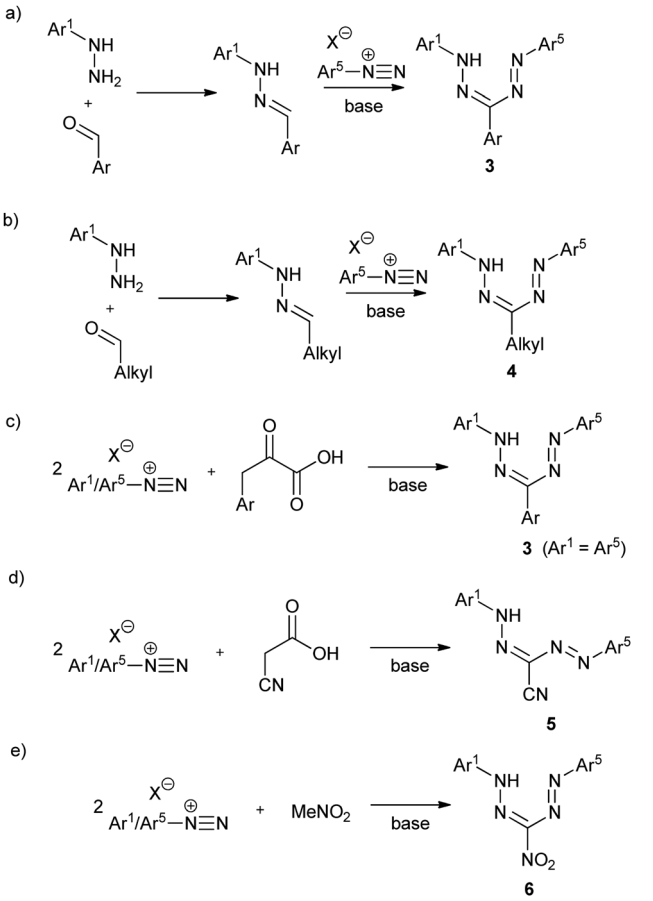

Scheme 1 Common routes for the synthesis of formazans.

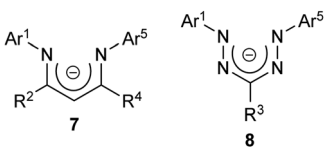

Chart 2

be somewhat surprising that the coordination chemistry of the anionic form of formazans, from this point forward referred to as formazanates **8** (Chart 2), has not been studied to the same extent.[3,18]

Formazanate ligands offer several unique and potentially useful traits when compared to related families of ligands. One important feature is their ability to engage in both oxidative and reductive redox chemistry due to the presence of high-lying filled (e^- donor) and low-lying empty (e^- acceptor) orbitals of π-symmetry (Fig. 2A). The ready availability of formazans with diverse substitution patterns (Scheme 1) allows rational tuning of the energies of these frontier orbitals. Both the HOMO and LUMO are mainly composed of orbitals centered on the NNCNN backbone, with additional contributions from the π-conjugated aromatic N-Ar^1/Ar^5 groups. Thus, the energies of both these orbitals should be sensitive to substituents at the *ortho*- and *para*-position of the *N*-aryl rings, primarily *via*

resonance effects. The LUMO is fully π-anti-bonding between the four nitrogen atoms in the formazanate framework and presents a nodal plane that runs through the C-R^3 fragment. As a result, structural variation at this position only has an inductive effect on the energy of the LUMO. In comparison to β-diketiminates and other related chelating N-donor ligands, the LUMO is low in energy, and compounds containing formazanate ligands may therefore be expected to readily engage in ligand-based reduction reactions (*i.e.*, formazanates are redox-active ligands).[19–21] Moreover, the low-lying π*-orbital gives rise to electronic transitions in the visible range of the spectrum, and both the absorption and emission properties of formazanate complexes are readily tunable by modifying the ligand structure. Finally, the coordinative flexibility that results from the four nitrogen atoms in the backbone allows for formation of four-, five- and six-membered chelates (Fig. 2B). In the symmetrical coordination modes (*i.e.*, with four- and six-membered chelate rings) the formazanate ligand backbones tend to exhibit bond lengths intermediate between single and double bonds of the respective atoms, indicating a high degree of electronic delocalization within the π-electron system. In the case of five-membered chelate rings, the metrical parameters in the formazanate backbone are often indicative of a more localized bonding picture although this appears to be dependent on the ligand substitution pattern and the nature of the central inorganic element.

The facile synthesis and unique attributes of formazans and formazanates has led to rejuvenated interest in their coordination chemistry over the past two decades. Herein, we provide a review of recent developments with focus on the reactivity and applications facilitated by this unique class of ligands. We have chosen to organize our review by group in the periodic table and begin with alkali metal complexes.

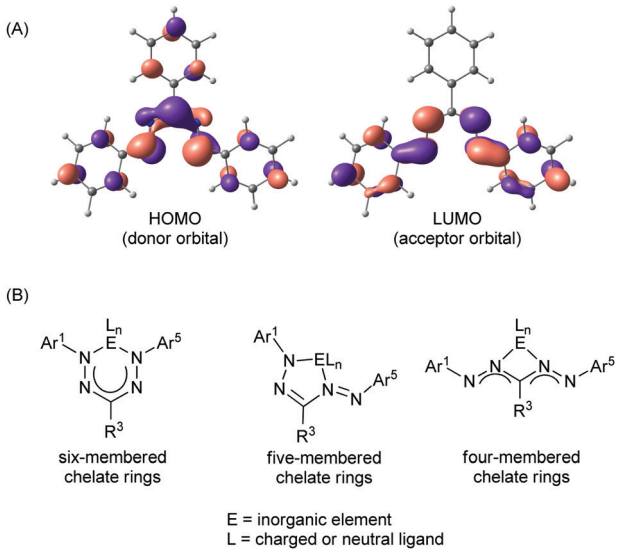

Fig. 2 (A) Frontier (Kohn–Sham) orbitals of the triphenylformazanate anion in the commonly observed 'closed' form, calculated using density functional theory (B3LYP/6-31G(d)). (B) Common coordination modes of formazanate ligands in inorganic complexes.

2. Formazanate coordination chemistry

2.1 Alkali metals (Na, K)

The deprotonation of formazans with strong alkali metal bases such as NaH or KH has been shown to cleanly generate the corresponding alkali metal formazanate salts (Scheme 2).[22] Three different formazans were studied, all with aromatic N-groups ($Ar^{1/5}$ = Ph, Mes) and substituents at the central C-atom (R^3) that were either a *p*-tolyl (**3a**), *t*-butyl (**4a**) or cyano moiety (**5a**). The molecular structures in the solid state, obtained by X-ray crystallography, demonstrate the flexibility of these ligands in their coordination behavior: both 4- and 5-membered chelate rings are accessible due to the presence of the four nitrogen atoms in the formazanate NNCNN backbone which allows the terminal as well as the internal N-atoms to interact with the metal center in a bidentate binding mode. This leads to solid state structures that range from dimeric (**9**) to hexameric (**10**) and polymeric (**11**) (Scheme 2, dashed lines indicate bonds that cause aggregation). In these ionic compounds, a high degree of π-delocalization is indicated by the equivalent N–N and C–N bond lengths within the ligand core, regardless of the chelate ring size. Cation exchange of the potassium salt **9** with [Bu_4N][Br] afforded the ion pair **12**. The crystal structure of **12** shows that, in the absence of a coordinating cation, the triarylformazanate anion adopts a linear arrangement. The solution structure of **9** was examined by variable-temperature NMR spectroscopy, which indicated that the dimeric structure is retained even in a donor solvent such as THF. These alkali metal salts are potentially useful reagents for the transfer of formazanate ligands to transition metals *via* salt metathesis reactions.

While alkali metal formazanate salts are stable when non-functionalized alkyl or aryl substituents are present, introduction of a C_6F_5 group as the R^3 substituent does not allow the synthesis of the corresponding formazanate salt by deprotonation. Instead, the nucleophilic formazanate anion $\mathbf{13}^-$ evolves by nucleophilic aromatic substitution (S_NAr) onto the *ortho*-position of the C_6F_5

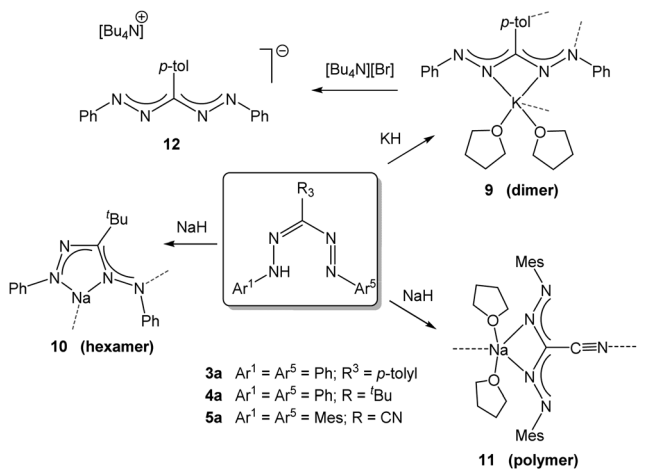

Scheme 2 Synthesis of alkali metal salts of formazanate ligands.[22]

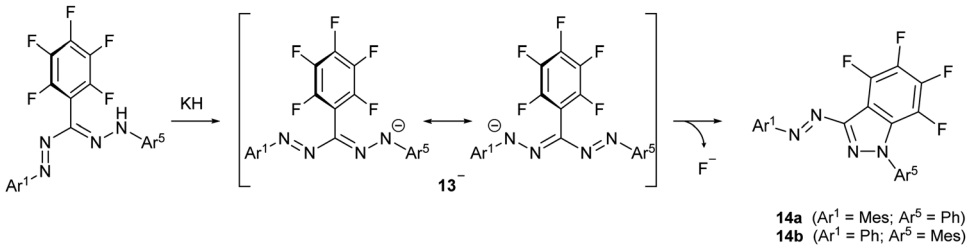

Scheme 3 S_NAr cyclization upon deprotonation of a 3-perfluorophenylformazan to give arylazoindazoles **14**.[23]

ring to give cyclization product **14** as a mixture of regioisomers (Scheme 3). The arylazoindazole **14** presents a novel heteroaromatic motif for azo photoswitches, and it was shown to have good photoconversion, thermal stability as well as fatigue resistance.[23]

2.2 Group 7 (Mn)

Formazanate complexes of group 7 metals have been reported only once in a 1998 report by the group of Brown with the preparation of the bis(benzothiazolylformazanate) manganese(II) complex **15**.[24] Compound **15** was obtained from the manganese(III) precursor $Mn(acac)_3$ by refluxing with formazan in EtOH under N_2 atmosphere (Scheme 4). The Mn(II) product likely arises from reduction by excess formazan, which in this process is oxidized to the corresponding tetrazolium salt. In the low-spin Mn(II) complex, the formazanate ligands are bound to the metal center in a *N*,*N*′,*N*″-tridentate fashion involving the benzothiazolyl substituent to give an octahedral coordination geometry. Formazanate complexes with the heavier congeners in group 7 have not been reported to the best of our knowledge.

2.3 Group 8 (Fe, Ru, Os)

Early work on Fe complexes with benzothiazolylformazanate ligands mirrors the results described above for Mn: treatment of Fe(III) salts with formazans leads to formation of low-spin octahedral Fe(II) complexes (**16**, Scheme 4), some of which were crystallographically characterized.[24–26] More recently, Hicks and co-workers reported an Fe(III) complex with a trianionic N_2O_2 ligand based on the formazanate scaffold, in which the *N*-aryl groups have an additional phenoxide O-donor moiety.[27] The low-spin Fe(III) complex **17** was obtained by salt metathesis from *in situ* generated Na-salt of the tetradentate N_2O_2 ligand with $FeCl_3$ (Scheme 5). Two additional pyridine ligands are

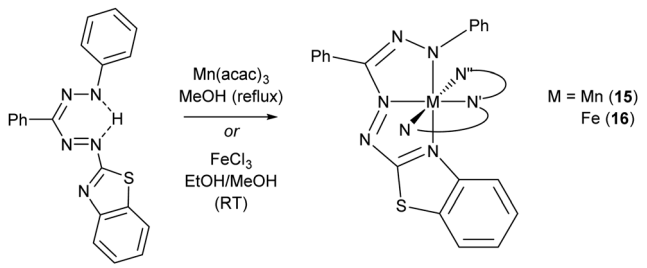

Scheme 4 Synthesis of homoleptic manganese(II) and iron(II) complexes with benzothiazolyl-substituted formazanate ligands (only one ligand shown in full, other abbreviated (*N*,*N*′,*N*″) for clarity).[24–26]

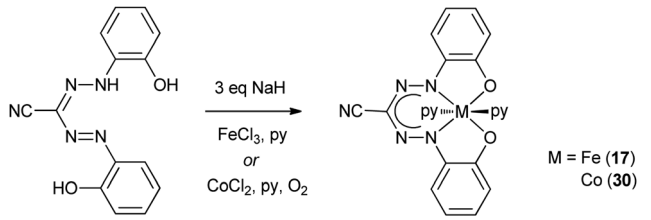

Scheme 5 Synthesis of Fe(III) and Co(III) complexes with trianionic N_2O_2 ligands based on the formazanate scaffold.[27]

bound *trans* to each other to give a pseudo-octahedral coordination geometry in **17**. Apparently, reduction to Fe(II) as discussed above does not occur in the synthesis of **17**,[24] which may be due to the presence of the additional anionic O-donor groups.

In 2016, the synthesis of the Fe(II) complex **18** with two simple, monoanionic triarylformazanate ligands was reported *via* salt metathesis using the potassium formazanate **9** (Scheme 6).[28] The absence of additional coordinating groups (*e.g.*, the benzothiazolyl substituent in compounds **16**) results in a four-coordinate environment around the iron center with the formazanate ligands bound *via* the terminal N-atoms. In contrast to the benzothiazolylformazanate complex **16**, the coordination mode of the formazanate ligands in compound **18** gives rise to six-membered chelate rings. The crystallographically determined solid-state structure of **18** showed a 'flattened' tetrahedral structure with very short Fe–N bond lengths of 1.8174(16)–1.8330(16) Å. Other remarkable features of this compound included its NMR and UV/vis spectra, which indicated a temperature-dependent equilibrium between a diamagnetic state ($S = 0$) at low temperature and a paramagnet ($S = 2$) at high temperature.

The unusual occurrence of spin-crossover in a four-coordinate complex was attributed to π-backdonation from the d^6 metal center to a low-lying formazanate π*-orbital, which stabilizes one of the high-energy orbitals and leads to an energy-ordering of the d-orbital manifold that has a 2-over-3 splitting (Fig. 3) that is reminiscent of that of six-coordinate, octahedral complexes (ligand-field 'inversion').[29] Cyclic voltammetry measurements for **18** showed quasi-reversible redox-events at −1.21 and −2.01 V (*vs.* $Fc^{0/+}$), which prompted attempts to synthesize and characterize these reduced species on a preparative scale. One-electron reduction of the Fe(II) complex **18** using one equiv. of Na/Hg as the reducing agent allowed the high-yield synthesis of the

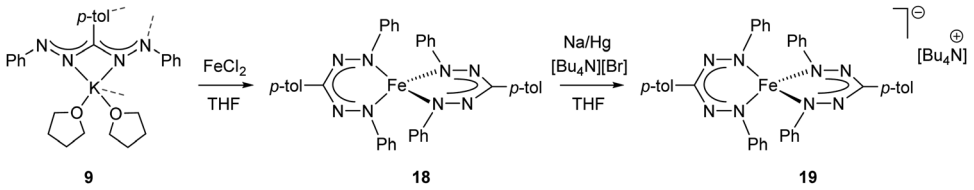

Scheme 6 Synthesis of bis(formazanate)iron(II) complex **18** and the corresponding one-electron reduction product **19**.[28]

anionic complex **19**. Analysis of structural (X-ray diffraction), spectroscopic (EPR, Mössbauer) and computational (DFT) data showed that **19** is best formulated as a low-spin (S = 1/2) Fe(I) complex containing closed-shell, monoanionic formazanate ligands. An alternative description in which reduction takes place at the ligand (with the additional electron in the low-energy formazanate π*-orbital) is not supported by the empirical data, despite the prominence of ligand-based reductions for these 'redox-active' ligands (see right).

The redox-active nature of the formazanate ligand in Fe(II) complexes was explored by the Holland group. Mono-formazanate iron amide **20** or its THF adduct **20-THF** were used to prepare the one-electron reduction product **21** (Scheme 7), which was studied using a variety of spectroscopic and computational techniques.[30] A multi-configurational quartet ground state was calculated for **21** using SORCI, which reproduces the empirical spectroscopic data. The calculations suggest two configurations to be dominant (*ca.* 25% contribution each). One of those represents a high-spin Fe(II) center that is anti-ferromagnetically coupled to a singly occupied ligand π*-orbital, whereas the other is best described as high-spin Fe(I) without ligand participation.

The reactivity of **21** towards alkyl iodides and I_2 was investigated, which suggested that formation of the reductive elimination product $IN(SiMe_3)_2$ occurred (at least formally) *via* a pathway that involves redox-reactions in the ligand (Scheme 7). $IN(SiMe_3)$ was also obtained directly from **20-THF** and I_2/NaI.

Another study from these authors examined the effect of the countercation on the structures and reactivity of a series of derivatives of **21**.[31] It was shown that when the countercation is one of the alkali metals (Na^+, K^+, Rb^+ or Cs^+), the compounds

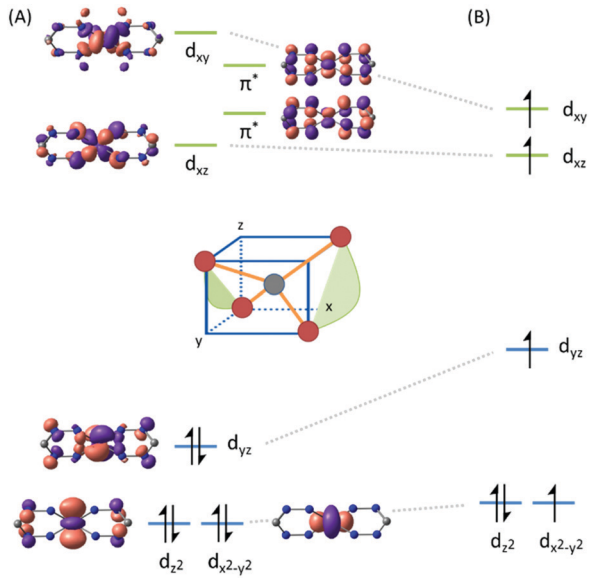

Fig. 3 DFT calculated frontier molecular orbitals in the low-spin (A) and high-spin state (B) of compound **18**. Reproduced from ref. 28 (https://pubs.acs.org/doi/10.1021/jacs.6b01552) with permission from the American Chemical Society. Further permissions related to the material excerpted should be directed to the ACS.

are dimeric in the solid state (**22a–d**, Scheme 7). In these dimers, the formazanate ligands coordinate in the 'open' form to give five-membered metallacycles, in which the 'pendant' terminal N-atom bridges to another Fe center. In contrast, sequestering the alkali cation with crown ether or allowing the dimers to equilibrate in THF solution results in monomeric

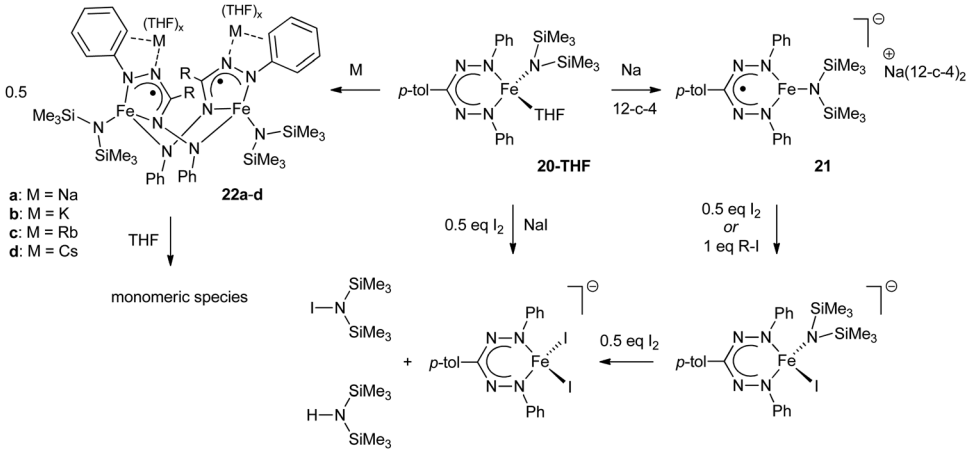

Scheme 7 Conversion of mono(formazanate)iron(II) amide complex **20-THF** to the one-electron reduction products **21** and **22**.[30,31]

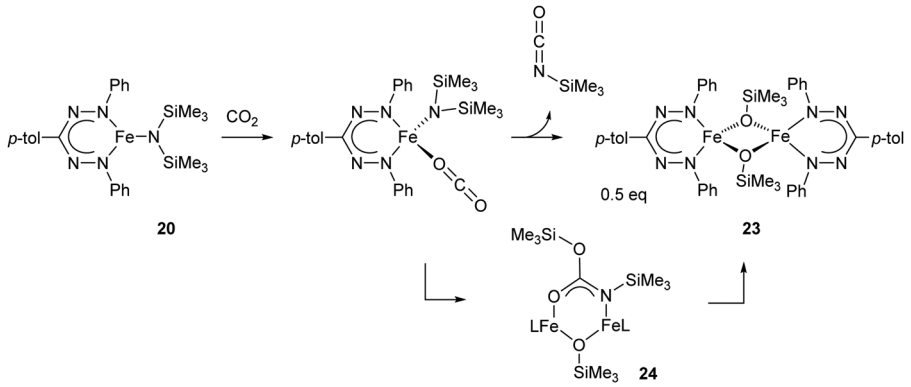

Scheme 8 Reaction of CO_2 and mono(formazanate)iron(II) amide complex **20** to form isocyanate.[32]

species in solution similar to **21** in which the formazanate ligand gives rise to a six-membered metallacycle.

The reactivity of the neutral complex **20** (or the THF-adduct **20-THF**) towards CO_2 was examined and shown to cleanly form isocyanate and the dimeric iron siloxide product **23** *via* the carbamate intermediate **24**, which was isolated from a low-temperature reaction and crystallographically characterized (Scheme 8).[32]

Mono(formazanate)iron(II) complexes with halide co-ligands are prone to ligand exchange reactions to the thermodynamically favored bis(formazanate) complexes (*e.g.*, **19**), but carrying out salt metathesis reactions in the presence of an additional equivalent of halide (such as $[Bu_4N][X]$) allows high-yield synthesis of four-coordinate ferrate complexes **25**.[33] The halide ligands in these complexes are labile, as demonstrated by the formation of octahedral, cationic complexes **26** upon treatment with isocyanide (Scheme 9a). Making use of its labile nature, **25** can be used as a source of three-coordinate Fe(II) and was shown to be an active catalyst for the synthesis of cyclic organic carbonates from CO_2 and epoxides, even in the absence of an external nucleophilic co-catalyst (Scheme 9b). It was proposed that the lability of a halide ligand in **25** allows binding of epoxide to the Lewis acidic Fe center, and the halide that is liberated acts as a nucleophile for the ring-opening of the epoxide to initiate the reaction.[34]

Formazanate complexes with the heavier elements in group 8 (Ru, Os) have only been sporadically investigated. Early work by Ibers and co-workers described the synthesis of complexes in which C–H activation of the NPh group took place to afford cyclometallated derivatives.[35] More recently, Lahiri *et al.* reported Ru complexes with a formazanate ligand and acetylacetonate, bipyridine or 2-phenylazopyridine co-ligands to give neutral complex **27** (Scheme 10a) and the cations $\mathbf{28}^+$ and $\mathbf{29}^+$,

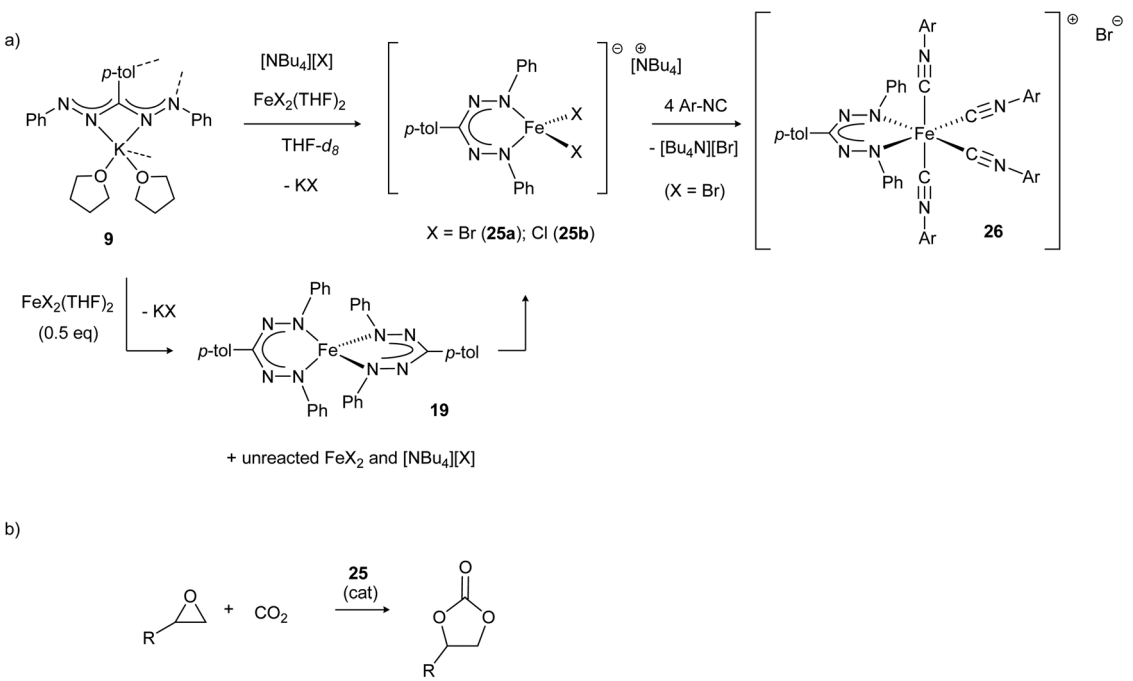

Scheme 9 (a) Synthesis of ferrate complexes **25** and subsequent halide exchange for isocyanide to give cationic complex **26**. (b) Application of **25** in the catalytic conversion of CO_2/epoxide to cyclic carbonates.[33,34]

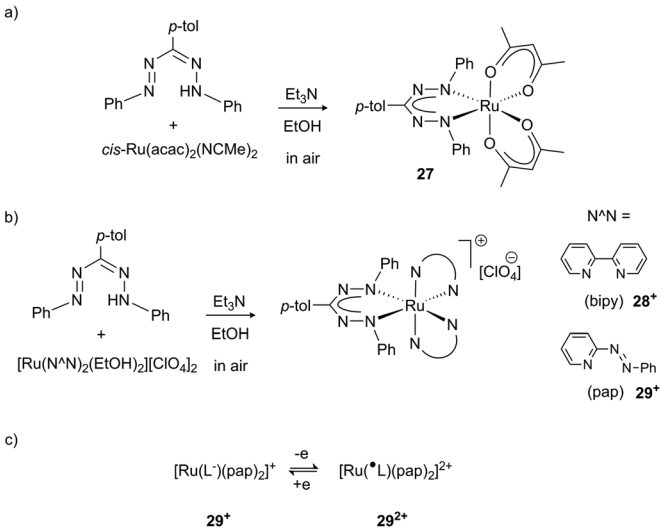

Scheme 10 Ruthenium complexes **27** and **28**$^{+}$/**29**$^{+}$ that show formazanate-based reduction and oxidation.[36]

respectively (Scheme 10b). These studies established bidirectional redox-noninnocence for the formazanate ligand: starting from complexes with a closed-shell monoanionic form of the ligand, both oxidation and reduction reactions were shown by spectroelectrochemisty and computational studies to occur in the formazanate moiety. This study provides the first evidence that the formazanate ligand can also bind in the neutral formazanyl radical form (L$^{\bullet}$ in the dicationic complex **29**$^{2+}$), thus extending the range of stable ligand oxidation states (Scheme 10c).[36]

2.4 Group 9 (Co, Ir)

In 2008, the Hicks group reported the preparation of the Co(III) complex **30** with a trianionic, tetradentate N_2O_2 cyanoformazanate ligand.[27] Compound **30** was obtained *via* salt metathesis with Co(II), followed by air oxidation, and was shown to be isostructural with Fe(III) complex **17** by X-ray diffraction (Scheme 5). Poddel'sky and co-workers reported triphenylformazanate cobalt complexes with one or two semiquinonate (SQ) ligands (**31**/**32**, Scheme 11).[37] The crystallographic, magnetic and spectroscopic data for these compounds indicates that the formazanate is bound as the closed-shell, monoanionic form of the ligand. The bidentate oxygen-ligands derived from 3,6-di-*tert*-butyl-*o*-benzoquinone (3,6-Q) are present as monoanionic semiquinonate radicals. Antiferromagnetic coupling, either between the S = 1/2 Co(II) center and a semiquinonate radical anion in **31** or between the two ligand radicals in the Co(III) complex **32**, leads to diamagnetic ground states for both compounds. In subsequent work, the authors examined the reduction chemistry of both cobalt complexes. These data suggest that in these compounds, reductions are ligand-based but occur in the quinone-derived ligand rather than in the formazanate to give a Co(II) product with closed-shell, dianionic catecholate ligand (**31**$^{-}$).[38] The corresponding one-electron reduction product **32**$^{-}$ is suggested to feature valence tautomerism (redox-isomerism) between Co(II) and Co(III) complexes with corresponding changes in oxidation state of the ligand (semiquinonate (SQ) and catecholate (Cat), respectively, see Scheme 11).[38]

Recent work from the Teets group has investigated a series of formazanate iridium(III) complexes with cyclometalated (C^N) ligands.[39] Both the substituent pattern on the formazanate as well as the nature of the C^N ligand were systematically varied to allow rational tuning of the electrochemical and optical properties of these octahedral Ir complexes. Stirring the dimeric bis-cyclometallated iridium chloride precursors with formazans at 80–85 °C in EtOH in the presence of NEt_3 afforded the formazanate complexes **33–36** in moderate to good yields (Scheme 12). The crude products are obtained as mixture of two isomeric products which differ in the coordination mode of the formazanate ligand. The metal center is coordinated either in a five- or six-membered chelate ring, which gives rise to complexes with C_1- or C_2-symmetry, respectively. The majority of these compounds could be obtained as a single isomer by recrystallization, and were shown by X-ray crystallography and NMR spectroscopy to

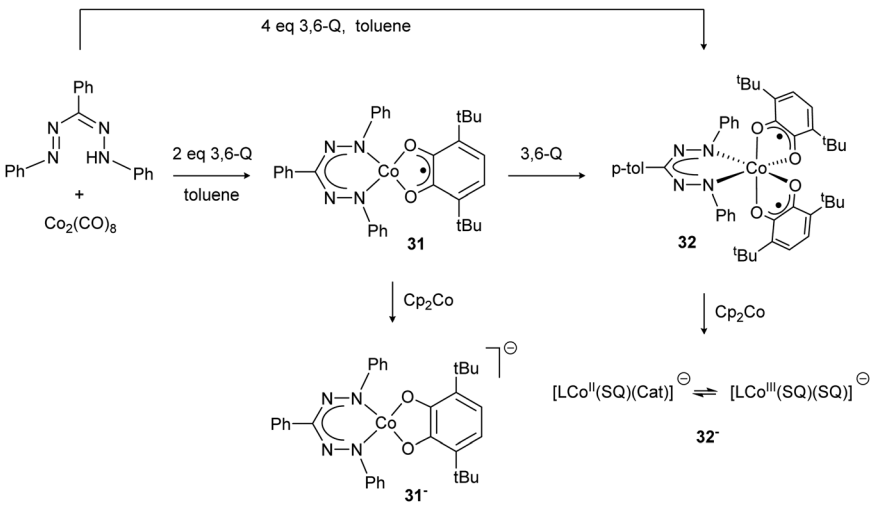

Scheme 11 Formazanate cobalt complexes with *o*-quinone-based co-ligands and their reduction chemistry.[37,38]

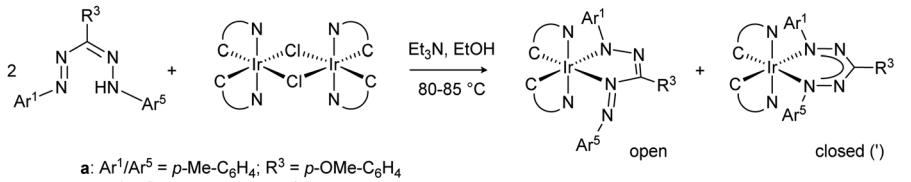

a: Ar^1/Ar^5 = *p*-Me-C_6H_4; R^3 = *p*-OMe-C_6H_4
b: Ar^1/Ar^5 = *p*-OMe-C_6H_4; R^3 = *p*-OMe-C_6H_4
c: Ar^1/Ar^5 = *p*-Me-C_6H_4; R^3 = *p*-CN-C_6H_4
d: Ar^1/Ar^5 = *p*-CN-C_6H_4; R^3 = *p*-Me-C_6H_4
e: Ar^1/Ar^5 = *p*-Me-C_6H_4; R^3 = CN
f: Ar^1/Ar^5 = *p*-CN-C_6H_4; R^3 = CN

33a-f: C^N = 2-phenylpyridine
34a-f: C^N = 2-(2,4-difluorophenylpyridine
35a,**b**,**e**,**f**: C^N = 2-phenylbenzothiazole
36a,**f**: C^N = 1-phenylisoquinoline

Scheme 12 Synthesis of iridium(III) formazanate complexes with cyclometalated C^N co-ligands.[39]

have a five-membered chelate structure ("open" form of the ligand). Only compounds **33b′** and **33c′** crystallized as the C_2-symmetric ("closed") isomer, whereas the isomers for compound **33a** could not be separated by crystallization or other means. Pure samples were shown to be kinetically stable: the other isomer that was present in the crude reaction mixture does not form upon heating $CDCl_3$ solutions to 60 °C. The different binding modes lead to a different degree of π-delocalization: the "open" isomers show alternating short/long bond lengths in the NNCNN core due to localized bonding, whereas the pairs of N–N and N–C distances are similar in the "closed" form. The preference for the "open" form of the ligand in these compounds stands in marked contrast to the symmetrical ("closed") binding mode that is commonly observed in formazanate transition metal complexes, and was attributed to a release of steric hindrance in the former. Analysis of the UV/vis absorption spectra for these compounds showed that there is little difference between the "open" and "closed" isomers, but that their intense, lowest-energy absorption (520–677 nm) due to a formazanate-based π→π* transition is sensitive to ligand substituent effects. Moreover, the absorption bands at higher energy (near-UV-visible) depend on the nature of the cyclometalated ligand, and are ascribed to metal-to-ligand charge transfer (Ir(d) → C^N(π*)). Cyclic voltammetry showed formazanate-centered reduction waves between −1.22 and −1.98 V *vs.* $Fc^{0/+}$ that were ascribed to reduction of the formazanate ligand. A second formazanate-based reduction was observed for several compounds, but this was generally not reversible and led to the appearance of additional oxidation waves upon the return scan. At more positive potentials (> −0.10 V *vs.* $Fc^{0/+}$), an oxidation wave was observed that is also quite sensitive to the formazanate substituents. Thus, while this may formally be assigned to a Ir(III)/Ir(IV) redox couple, there is also a significant formazanate-contribution to the HOMO in these compounds.

2.5 Group 10 (Ni, Pd, Pt)

Reports published since 2000 on nickel complexes with formazanate ligands have established detailed insight in the structures and properties of these compounds, and applications are starting to emerge. In 2006, the group of Vatsadze unambiguously confirmed the symmetrical, six-membered chelate structure for the bis-(triphenylformazanate)nickel complex **37a**,[40] which had been known since 1941[41] (the crystal structure of a related 3-Me substituted derivative was reported in 1967).[42] Bis(formazanate)-nickel(II) complexes have square planar coordination geometries and thus are diamagnetic. The metal ion is displaced out of the ligand plane to minimize steric interactions between the N-Ar groups. Derivatives with pyridine substituents on the formazanate backbone were prepared as potential metalloligands in supramolecular chemistry (**37b–d**, Scheme 13a).[40] Tezcan and co-workers reported related Ni complexes, and studied the effect of ligand substituents on the spectroscopic and electrochemical properties.[43] Zaidman *et al.* prepared a series of bis(formazanate) nickel complexes from formazans with various (heteroaromatic) substituents or linked bis-formazan scaffolds, and studied their catalytic activity in ethylene oligomerization (for representative structures **38**/**39**, see Scheme 13b).[44] Upon treatment with $AlEtCl_2$, the complexes showed some catalytic activity towards the formation of a mixture of butenes, hexenes and octenes, but also resulted in substantial amounts of (poly)ethyltoluenes by Friedel–Crafts alkylation of the toluene solvent with ethylene.

Nitro- or cyanoformazans were used by Hicks *et al.* to prepare the nickel complexes **40** and **41** (Scheme 14).[27] While cyanoformazans reacted with $Ni(OAc)_2$ to produce ill-defined (oligomeric/polymeric) products due to coordination of the cyano group, nitroformazans led to bis(formazanate)Ni complexes when small *N*-aryl substituents are used (*e.g.*, Ar^1/Ar^5 = *p*-tolyl). On the other hand, sterically more demanding substituents (2,6-Me_2 substituted aromatic rings) prevented formation of homoleptic complexes and instead led to mono(formazanate) nickel hydroxides, which are dimeric in the solid state (Scheme 14b).

Palladium complexes **42** with nitroformazanate and fluorinated acetylacetonate ligands (Scheme 15a) were prepared and their electrochemical properties evaluated.[45] The irreversible reductions observed in the cyclic voltammograms led the authors to conclude that the radical dianionic ligand that is generated is not stable in these 'metalaverdazyl'-type palladium complexes.

Formazanate palladium complexes **43** with heteroaromatic substituents were reported by Lipunova *et al.* (Scheme 15b).[46] Starting from $PdCl_2$, several complexes were obtained with the empirical formula (formazanate)PdCl that show intense absorption maxima in the near-IR range (820–1020 nm). Although the structure of these compounds remains unknown, a Cl-bridged dimeric structure was suggested based on the mass spectrum. Addition of amine bases results in loss of the near-IR band and appearance of a new absorption in the visible

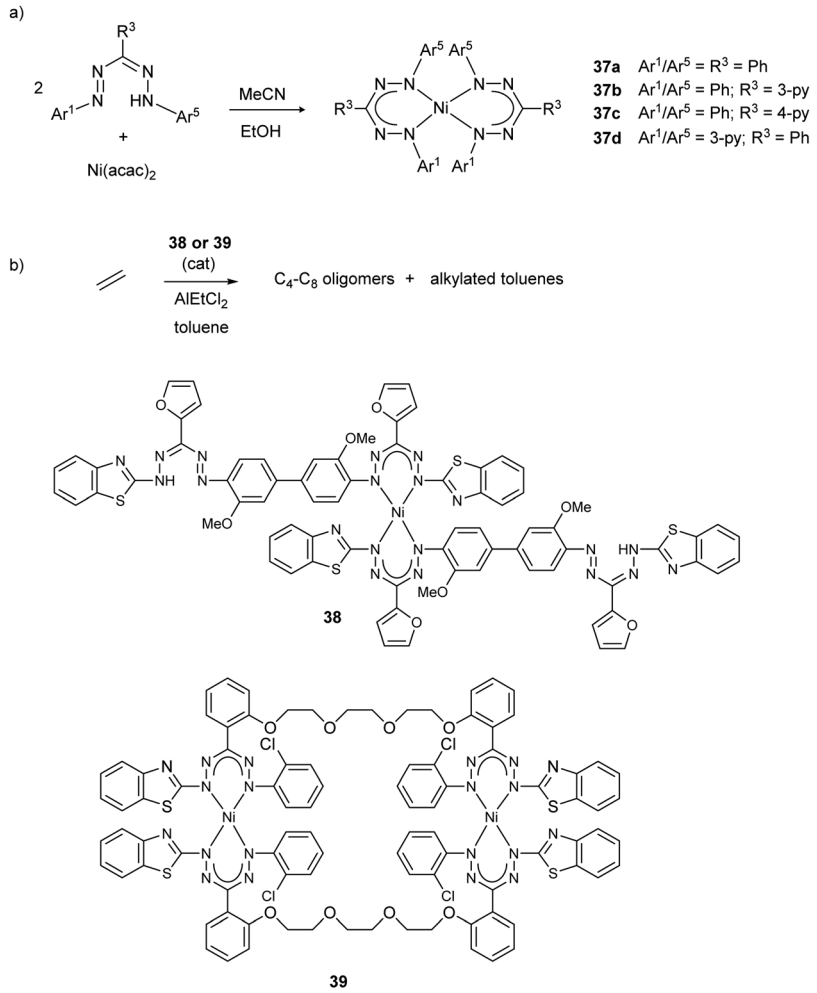

Scheme 13 (a) Synthesis of square planar nickel complexes with triarylformazanate ligands. (b) Representative structures of nickel complexes described by Zaidman *et al.*, and their application as catalysts for ethylene oligomerization.[40–44]

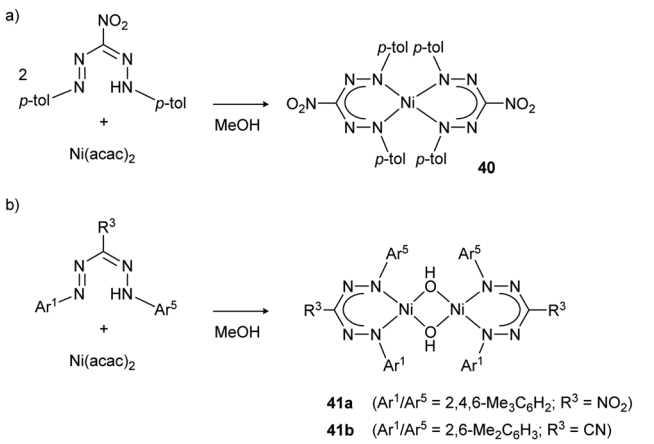

Scheme 14 (a) Synthesis of homoleptic bis(formazanate) nickel complex **40**. (b) Synthesis of heteroleptic cyano/nitro-formazanate nickel hydroxide complexes **41** with larger *N*-aryl groups.[27]

range (630 nm). The product after treatment with $[NH_4][OH]$ was identified as a dimeric palladium species (**44**) by using single-crystal X-ray diffraction.

The synthesis of organometallic mono(formazanate) palladium complexes with a Pd–Me bond was described by the groups of Otten and Milani (Scheme 16).[47] Salt metathesis between potassium formazanate and the palladium precursor $(COD)Pd(CH_3)Cl$ in THF was unsuccessful due to the poor stability of the putative three-coordinate complex $(formazanate)Pd(CH_3)$. From these reactions, the corresponding homoleptic bis(formazanate) palladium complex was invariably obtained (a closely related compound was described previously by Siedle).[48] However, addition of an equivalent of $[Bu_4N][Cl]$ to the reaction mixture afforded the four-coordinate palladate complex **45**, in which the halide ligand is labile and thus allows binding of unsaturated substrates. Insertion of CO, isocyanide and methyl acrylate into the Pd–CH_3 bond was demonstrated, but less reactive olefins (ethylene, styrene) did not react.

The properties of platinum formazanate complexes **46–49** with cyclometallated ligands were studied by Teets and co-workers with a wide range of ligand substituents (Scheme 17a).[49,50] Formazanate coordination to the platinum center was shown by a combination of spectroscopic, electrochemical and computational studies to lead to substantial changes in comparison to the free ligands, with absorption maxima that are red-shifted to *ca.* 660 nm. In addition

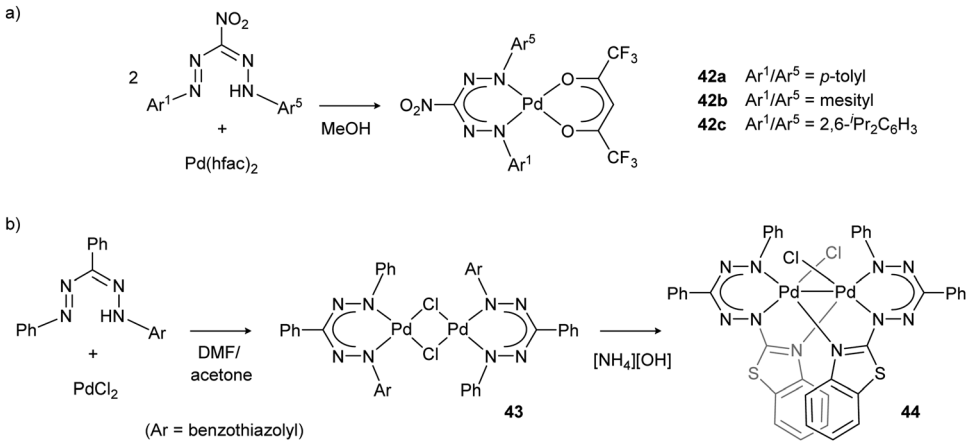

Scheme 15 (a) Synthesis of nitroformazanate palladium complex **42** with fluorinated acetylacetonate ligands. (b) Synthesis of binuclear Pd–Pd bonded complex **44** *via* the chloride-bridged dimer **43**.[45,46]

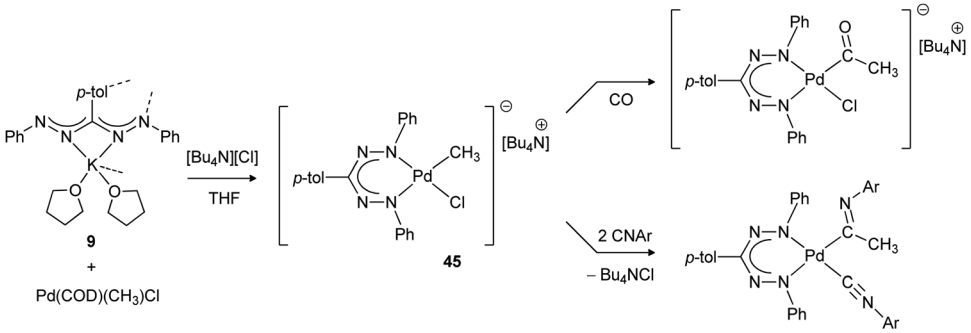

Scheme 16 Synthesis of organometallic mono(formazanate) palladium complex **45** and subsequent insertion reactions with unsaturated substrates.[47]

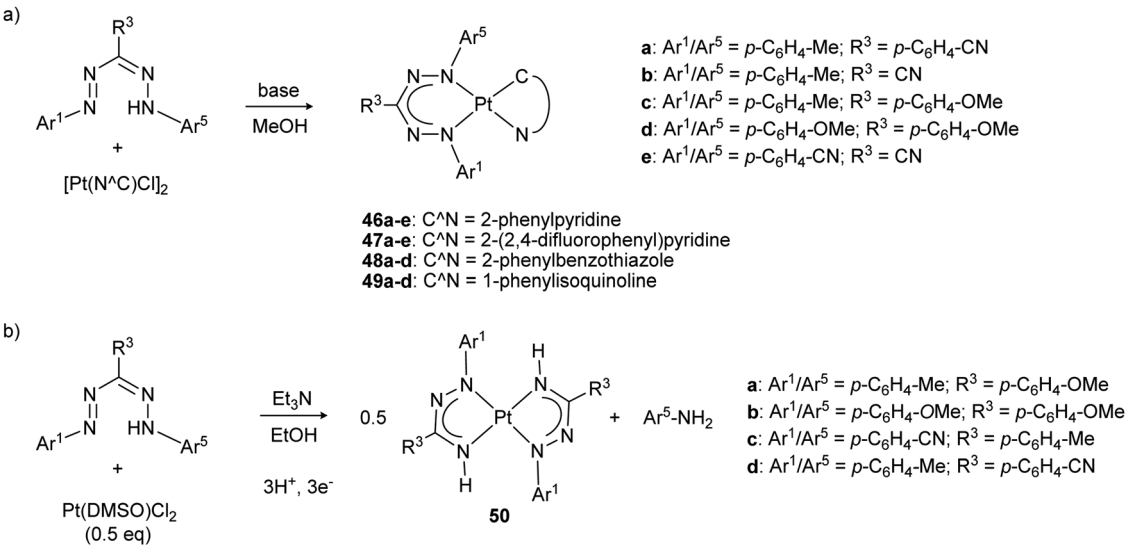

Scheme 17 (a) Synthesis of square planar platinum complexes with formazanate and cyclometallated C^N ligands. (b) Synthesis of homoleptic platinum azoiminate complexes *via* reductive N–N bond cleavage.[49–51]

to the typical ligand π → π* transition, a (minor) contribution of Pt(d) → formazanate charge transfer character is observed in the excited state. Computational data indicate that both the HOMO and LUMO are primarily ligand-based, and spectroelectrochemical data support the notion that ligand-based one-electron reductions take place at relatively accessible potentials between −1.2 and −1.6 V *vs.* $Fc^{0/+}$. Compounds **46e**/**47e** (with highly electron-withdrawing ligands) are exceptions and show even more facile

reductions at −0.84 and −0.80 V *vs.* $Fc^{0/+}$, respectively. A second reduction occurs at more negative potentials (∼−2 V *vs.* $Fc^{0/+}$), and both these reduction waves were assigned to formazanate-based processes. Both reduction waves respond in a similar manner to the presence of electron-donating/withdrawing substituents on the formazanate ligands, resulting in a relatively constant separation between these two of *ca.* 0.6–0.7 V. A third cathodic wave (<−2.3 V) was assigned to reduction of the Pt–C^N fragment. Moreover, irreversible oxidations were also observed at mild potentials (around +0.1 V *vs.* $Fc^{0/+}$). Despite the rather large variation of the LUMO energy levels, with first reduction potentials differing by as much as 0.79 V across the series, the electronic spectra show rather similar absorption maxima in the visible range (λ_{max} = 600–665 nm, a range of *ca.* 0.2 eV). Apparently, both the HOMO and LUMO energy are affected to approximately the same extent by substituent effects, a feature that is in line with the computed frontier orbital compositions of formazanate ligands (Fig. 2, see also Section 2.8.1).

Changing the platinum precursor from a cyclometallated species (*e.g.*, $[Pt(C^N)Cl]_2$) to $Pt(DMSO)Cl_2$ under similar reaction conditions to those used for the synthesis of **46–49** led to reductive cleavage of the formazan N–N bond to give azo-iminate complexes **50** (Scheme 17b).[51] Although the mechanism for this overall $3H^+/3e^-$ transformation is not fully understood, control experiments indicated that the solvent (MeOH, EtOH) is likely involved as the source of protons and electrons. On the one hand, this study highlights that the reactivity of formazans can be utilized to form organic ligands that are otherwise difficult to access (*e.g.*, azo-iminates). On the other hand, it shows that reductive N–N bond cleavage is a potential decomposition reaction for formazanate complexes in reduced states, albeit that a general understanding of this type of reactivity remains to be established.

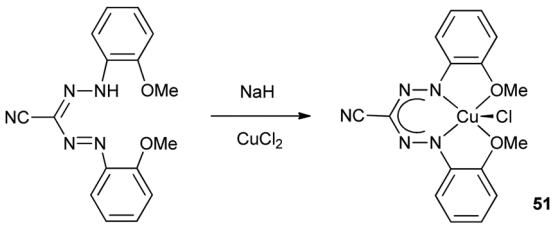

Scheme 18 Synthesis of Cu(II) complex **51** with tetradentate, monoanionic N_2O_2 formazanate ligand.[27]

2.6 Group 11 (Cu)

The Hicks group reported the copper formazanate complex **51** in which both *N*-aryl substituents carry an additional –OMe donor functionality (Scheme 18).[27] The solid state structure of the complex was determined by X-ray crystallography, which showed a pseudo-five-coordinate geometry around the Cu center. One of the OMe groups is clearly bonded with a Cu–O distance of 2.068(2) Å, whereas the other is significantly further away at 2.479(2) Å. Magnetic and spectroscopic characterization confirmed the presence of a $S = 1/2$ Cu(II) center with the unpaired electron in the $d_{x^2-y^2}$ orbital ($g_{\parallel}$ = 2.174 and $g_{\perp}$ = 2.064).

The unusual electronic features of formazanate ligands were explored in the context of Cu(I)-mediated dioxygen activation. Hicks, Tolman and co-workers evaluated the reactivity of a mononuclear Cu(I) complex **52**, which is coordinated by a sterically demanding nitroformazanate ligand with *N*-2,6-diisopropylphenyl substitution pattern (Scheme 19).[52,53] The ligand was shown to be similar in its electron-donating properties to electron-poor CF_3-substituted β-diketiminate ligands by comparing oxidation potentials and CO stretching frequencies. Reaction of **52** with O_2 at room temperature afforded the bis(μ-hydroxo)dicopper(II) complex **53**. Performing the reaction at −80 °C, however, allowed identification of an intermediate that was assigned as the bis(μ-oxo)dicopper complex **54-i**. Characterization of this intermediate by UV/vis spectroscopy showed that the nature of the electronic transitions in the formazanate and β-diketiminate complexes are markedly different. The low-energy transition (λ_{max} = 525 nm) observed for **54-i** was shown by DFT calculations to have substantial contribution from orbitals on the formazanate framework (Scheme 19). In contrast to the β-diketiminate analogues, decay of the initial oxygenation product **54-i** at temperatures above −50 °C showed the formation of a second intermediate

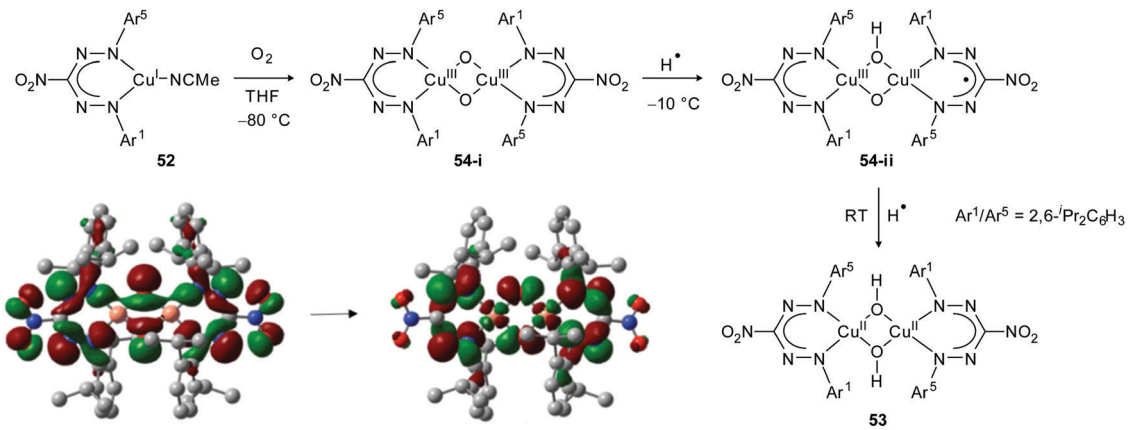

Scheme 19 Reaction of formazanate Cu(I) complex **52** with O_2. Donor and acceptor Kohn–Sham orbitals involved in the lowest-energy electronic transition in intermediate **54-i** are adapted from ref. 52 with permission from the American Chemical Society.

(**54-ii**) en route to the bis(μ-hydroxo)dicopper(II) end-product **53**. The spectroscopic features of **54-ii** (UV/vis: λ_{max} = 724 nm; X-band EPR at 4 K: isotropic signal at $g \sim 2.0$) led the authors to suggest that this species is formed by hydrogen-atom abstraction from the solvent by the $Cu(III)_2O_2$ core and contains an organic (ligand) radical. The product of this $H^{\bullet}$ transfer, formally containing a Cu(II)Cu(III)(OH)(O) moiety, presumably undergoes electron-transfer from Cu(II) to the formazanate ligand and forms the dicopper(III) complex **54-ii** with a radical dianionic formazanate ligand. An alternative description based on a coordinated neutral formazanyl radical was considered less likely due to the similarity of the spectroscopic features of **54-ii** with those observed for other compounds containing radical dianionic formazanate ligands.

2.7 Group 12 (Zn)

Although ligands based on the formazanate NNCNN framework have a long history in the spectrophotometric quantification of zinc and copper ions (Zincon),[54] reports from recent years have provided a better understanding of the properties of formazanate zinc complexes, with a specific focus on the ability of formazanates to function as electron-reservoirs (*i.e.*, as redox-active ligands). In 2014, the synthesis of bis(formazanate) zinc complexes **55a/b** was described *via* protonolysis using $ZnMe_2$ (Scheme 20), and the properties of these compounds were explored by cyclic voltammetry and chemical synthesis.[55]

Two quasi-reversible, single-electron redox processes were observed in the voltammogram of **55a** at −1.31 and −1.55 V *vs.* $Fc^{0/+}$ that correspond to the redox-couples $\mathbf{55a}^{0/-}$ and $\mathbf{55a}^{-/2-}$, respectively. Qualitatively similar data were obtained for the 3-*tert*-butyl formazanate complex **55b**, but a cathodic shift (to −1.57/−1.85 V *vs.* $Fc^{0/+}$) was observed due to the presence of the electron-donating ^{t}Bu substituent. The stability of the one- and two-electron reduced species on the electrochemical timescale prompted the chemical synthesis of these compounds. Addition of one equivalent of Na/Hg reducing agent to THF solutions of **55a/b** afforded the corresponding radical anions $\mathbf{55a/b}^{\bullet-}$, respectively, which were characterized by X-ray crystallography. In these radical anionic complexes, the Na^+ countercation interacts with the nitrogen atoms in the ligand backbone. The two formazanate ligands around the zinc center were shown to be different, with one having intraligand metrical parameters that are very similar to the neutral starting materials whereas the other ligand (where the cation is bound) shows substantially elongated N–N bonds (avg. 1.304 Å in **55a** *vs.* 1.363 Å in $\mathbf{55a}^{\bullet-}$). It was concluded that the latter ligand is present as a radical dianion, *i.e.*, in the metallaverdazyl form. Treatment of **55a/b** with 2 equiv. of Na/Hg was shown to form the corresponding dianionic complexes ($\mathbf{55a/b}^{2-}$), in which both ligands are present as radical dianions bonded to a Zn^{2+} center, as demonstrated by the crystal structure for $\mathbf{55b}^{2-}$ (Fig. 4A), which shows all N–N bonds being elongated (>1.355 Å). The EPR features of $\mathbf{55}^{2-}$ at 77 K in frozen THF solution are consistent with a triplet organic diradical, with g = 2.0028 and a zero-field splitting parameter $D \approx 11.5 \times 10^{-3}$ (Fig. 4B). A variable-temperature EPR study suggested that although the triplet state is apparently significantly populated at 77 K, $\mathbf{55a}^{2-}$ has an unusual singlet biradical electronic ground state. This was confirmed by broken-symmetry DFT calculations (Fig. 4C). The presence of radical dianionic ligands in the reduced compounds was furthermore confirmed by UV/vis spectroscopy, which showed features typical for verdazyl-type radicals (low-energy absorptions at $\lambda > 750$ nm, Fig. 4D).

The influence of formazanate substitution pattern on the structure and electronic properties of the resulting bis(formazanate) zinc complexes was investigated by X-ray crystallography, cyclic voltammetry and UV/vis spectroscopy.[56] The majority of the compounds **55a–g** have the formazanate ligands bound in a six-membered chelate ring, but when the *N*-aryl substituents are electronically dissimilar the π-delocalization is less pronounced and five-membered chelate rings become energetically accessible. For example, compound **55f** (Ar^1 = Mes; Ar^5 = C_6F_5) was found to have one ligand bound in the unusual 'open' geometry (*via* both a terminal and internal N-atom) whereas the other is present in the

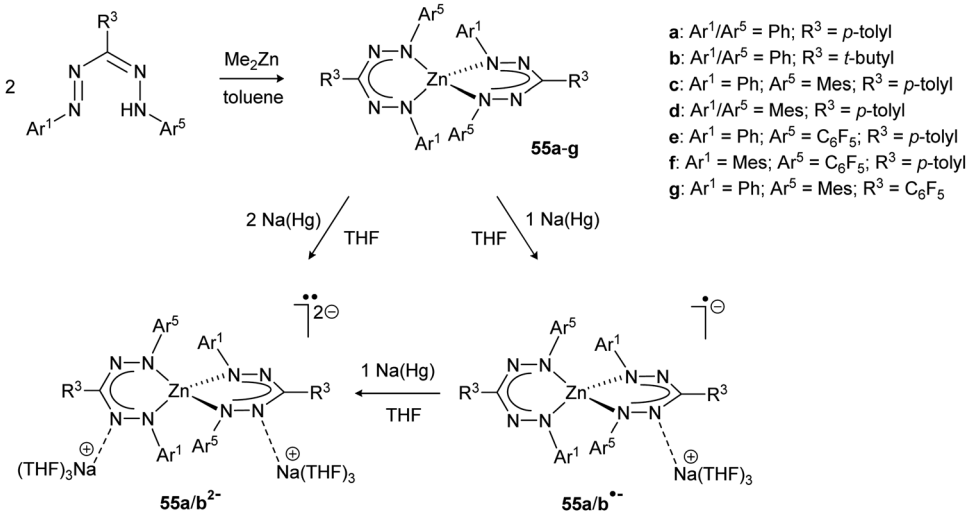

Scheme 20 Synthesis of bis(formazanate) zinc complexes **55**, and subsequent reduction to the corresponding radical anions $\mathbf{55}^{\bullet-}$ and dianions $\mathbf{55}^{2-}$.[55,56]

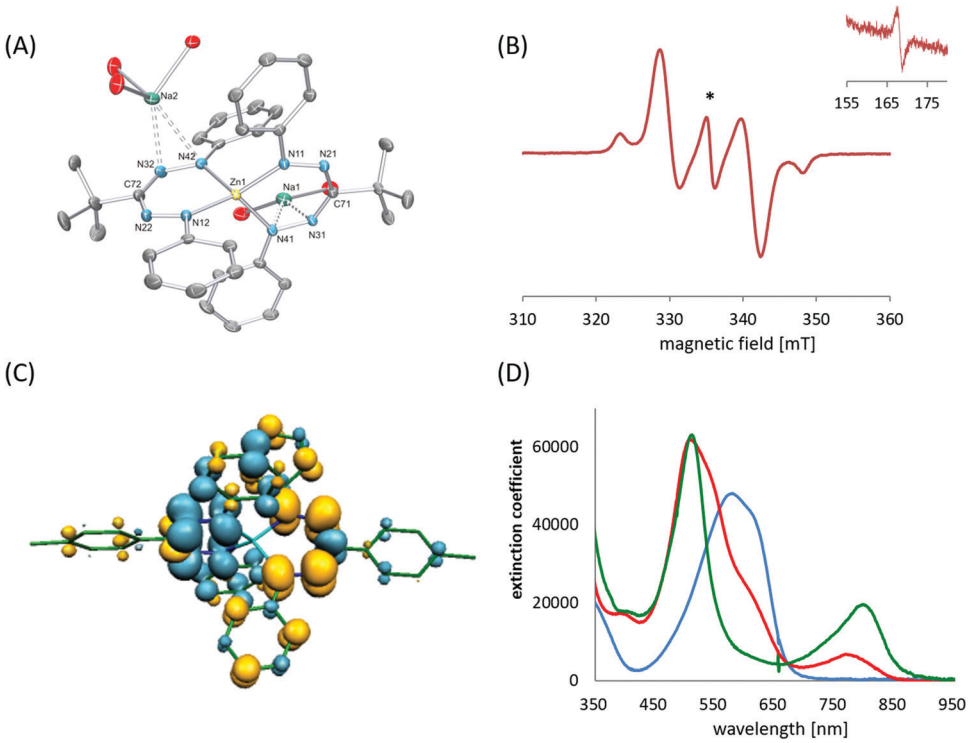

Fig. 4 Molecular structure of **55b**$^{2-}$, with hydrogen atoms and coordinated THF molecules (except the O-atoms) omitted for clarity (A). EPR spectrum of **55a**$^{2-}$ recorded at 77 K in frozen THF solution (B); asterisk denotes doublet impurity, inset shows half-field region). Spin density plot for the broken-symmetry DFT calculations on **55a**$^{2-}$ (C). UV-vis spectra for **55a** (blue), **55a**$^{\bullet-}$ (red) and **55a**$^{2-}$ (green) in THF solution (D). Adapted from ref. 55 with permission from John Wiley and Sons.

more common 'closed' form. Solution NMR studies indicated a dynamic equilibrium between these isomers. It was found that the redox-potentials vary in a predictable manner based on the electron-donating/withdrawing ability of the substituents, and one-electron reduction potentials that span a wide range (between −1.17 to −1.86 V *vs.* $Fc^{0/+}$) were demonstrated. Gilroy and co-workers have examined in more detail these substituent effects, and correlated the optoelectronic properties of formazanate boron difluoride compounds with computed frontier molecular orbitals (see Section 2.8.1). In addition to reduction waves corresponding to the formation of the radical anions **55**$^{\bullet-}$ and diradical dianions **55**$^{2-}$, the voltammograms indicated that these compounds can be further reduced at more negative potentials (<−2.5 V *vs.* $Fc^{0/+}$). Although the stability of these highly reduced species is limited, the observation that five different oxidation states are accessible in these simple compounds (*i.e.*, ranging from neutral **55** to the tetranion **55**$^{4-}$) is noteworthy and suggests that each formazanate ligand can be reduced by up to two electrons. This study furthermore demonstrated that bis(formazanate) zinc complexes with two different formazanate ligands are accessible in a stepwise manner (*e.g.*, **56**, Scheme 21a), and provided the first example of a zinc complex with a parent (neutral) formazan ligand when the less basic reagent $Zn(C_6F_5)_2$ was used (**57**, Scheme 21b).

2.8 Group 13 (B, Al, Ga, In)

2.8.1. Synthesis and reactivity of boron difluoride adducts. Arguably the most widely studied family of formazanate coordination compounds over the past two decades are adducts of four-coordinate boron. Hicks and co-workers generated interest in this class of molecular materials when they converted triarylformazans **3** to boron diacetato complexes of formazanate ligands **58** and showed that they could be converted to verdazyl-type radical anions **58**$^{\bullet-}$ (Scheme 22) that were stable enough in the solid state to be identified by UV-vis absorption (λ_{max} ∼ 740 nm) and EPR spectroscopy (broad isotropic signal, g ∼ 2.00).[57] This work set the stage for future research conducted by the teams led by Otten and Gilroy nearly a decade later, leading to the exploration of the chemistry and application of a wide range of boron formazanate complexes.

Inspired by the rich chemistry of boron difluoride (BF_2) adducts of chelating N-donor ligands,[58] including boron dipyrromethenes (BODIPYs),[59,60] the first examples of BF_2 formazanates **59** were synthesized from the corresponding homoleptic Zn(II) complexes **55** (Scheme 23a).[61] The resulting complexes, which benefited from structural rigidity and stability associated with the 'BF_2^+' fragment, could be electrochemically reduced in two steps to the corresponding radical anions and dianions. Chemical reduction with cobaltocene ($CoCp_2$) afforded the first structurally characterized examples of radical anions supported by boron adducts of formazanates, which showed characteristic elongation of the formazanate N–N bonds from an average of *ca.* 1.309 Å for **59a** to 1.362 Å for **59a**$^{\bullet-}$ due to the population of the LUMO, which possesses N–N antibonding character (Scheme 24).[61] An alternative synthesis involving the conversion

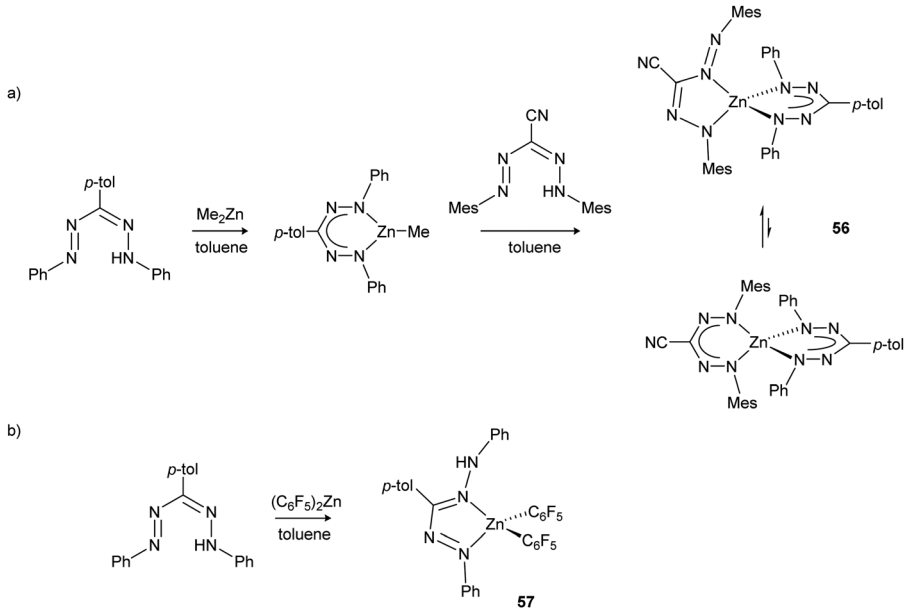

Scheme 21 (a) Synthesis of bis(formazanate) zinc complexes **56** with two different formazanate ligands. (b) Synthesis of formazan complex **57** using the less basic reagent $Zn(C_6F_5)_2$.[56]

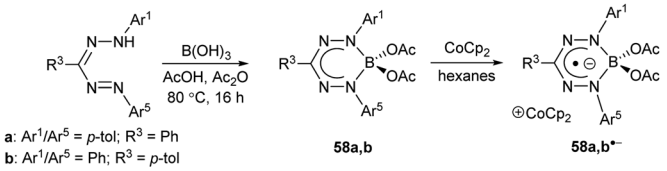

Scheme 22 Synthesis of boron diacetate complexes of formazanate ligands and their corresponding radical anions.[57]

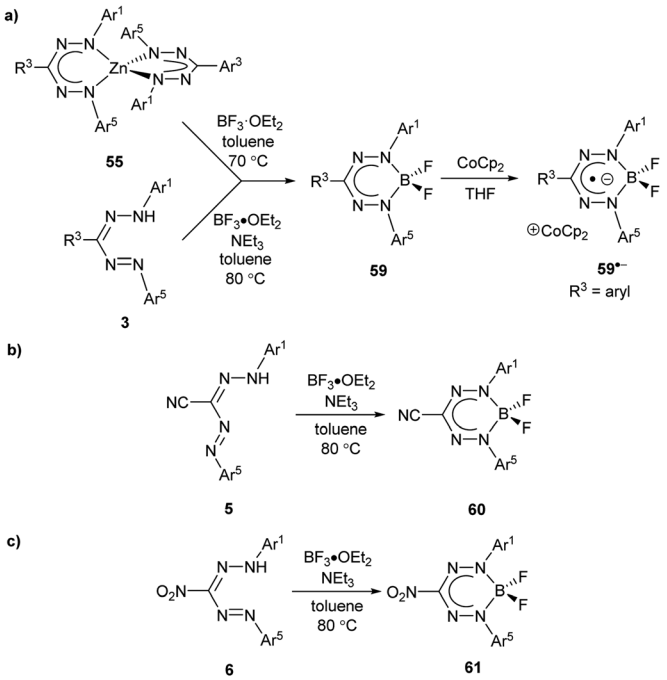

Scheme 23 Synthetic routes to boron difluoride complexes of (a) triarylformazanate ligands (and corresponding radical anion), (b) 3-cyanoformazanate ligands, and (c) 3-nitroformazanate ligands.[61–64]

of 3-cyanoformazans **5** to BF_2 complexes **60** by heating toluene solutions containing excess NEt_3 and $BF_3{\cdot}OEt_2$ at 80 °C overnight was published[62] soon after the initial report (Scheme 23b) and was later extended to 3-aryl (**3**)[63] and 3-nitroformazans (**6**)[64] to produce BF_2 complexes **59** and **61** (Scheme 23a and c). The 3-cyano and 3-nitro derivatives could also be electrochemically reduced in two steps, and were also the first examples of BF_2 formazanate dyes to exhibit appreciable photoluminescence.

As noted earlier, BF_2 formazanate complexes can be electrochemically reduced in two one-electron steps. These reduction events occur at $E_{red1} \sim -0.8$ and $E_{red2} \sim -1.9$ V relative to the $Fc^{0/+}$ redox couple for adducts of triarylformazanates (**59**),[63,65] $E_{red1} \sim -0.6$ and $E_{red2} \sim -1.7$ V for 3-cyanoformazanates (**60**),[62] and $E_{red1} \sim -0.5$ and $E_{red2} \sim -1.6$ V for 3-nitroformazanates (**61**)[64] bearing phenyl substituents at the 1,5 position of the ligand backbone. There are a number of reagents that could potentially reduce BF_2 formazanates to their radical anion forms, including $CoCp_2$ and its permethylated analogue ($CoCp^*_2$), which are both 19-electron metal complexes.[66] However, relatively few reducing agents are strong enough to generate the dianion form of BF_2 formazanates.[66] The isolation of the dianion form of BF_2 formazanates was attempted using a Na/Hg amalgam as a chemical reductant (Scheme 24).[67] Treatment of complex **59a** with two equiv. of Na/Hg resulted in the production of novel, crystallographically-characterized BN heterocycles **62–65**, whose formation was driven by the production of NaF and likely implicates B(I) carbenoid intermediates **66** and **66′**. Treatment of heterocycles **62** and **63** with XeF_2 resulted in the regeneration of BF_2 complex **59a** in high yield.

Attempts to exploit the chelate effect toward the isolation of complex **67** from the potentially tetradentate formazanate ligand 1,5-bis(2-hydroxyphenyl)-3-cyanoformazan resulted in the production of a number of unprecedented BN heterocycles

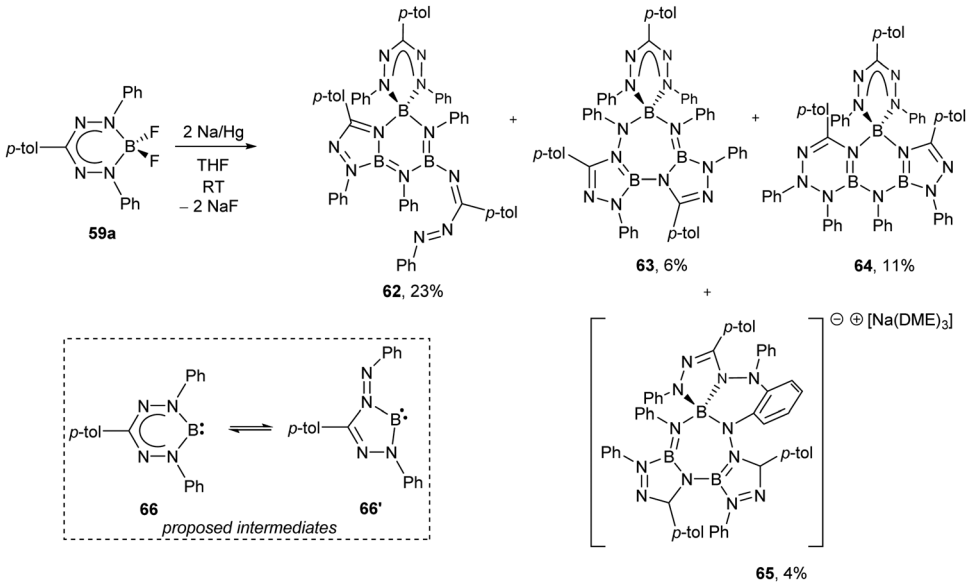

Scheme 24 Synthesis of novel BN heterocycles **62–65** *via* treatment of BF_2 formazanate **59a** with Na/Hg amalgam and proposed B(I) carbenoid intermediates **66** and **66′**.[67]

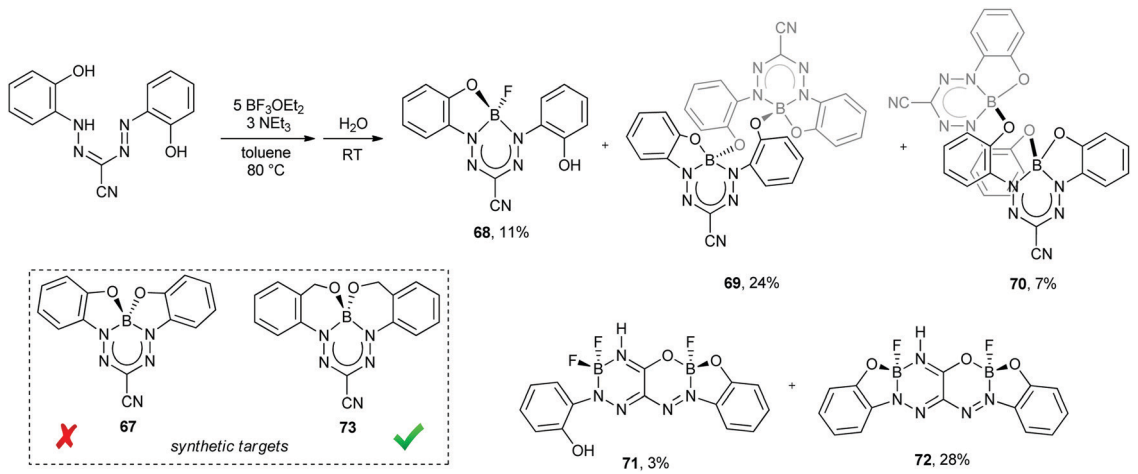

Scheme 25 Synthesis of unusual BN heterocycles **68–72** from a potentially tetradentate $N_2O_2^{3-}$ formazanate ligand and synthetic targets **67** and **73**.[68]

68–72 (Scheme 25).[68] The absence of **67** in the resulting reaction mixtures can be attributed to ring strain associated with the 5-membered BOCCN chelate rings that would need to form during its synthesis. This hypothesis was supported by the fact that switching from phenol to benzyl alcohol *N*-aryl substituents resulted in the clean formation of **73**, which involved only the formation of 6-membered BOCCCN chelate rings, which impose a lesser degree of ring strain. Compounds **68–72** were isolated from crude reaction mixtures through the use of column chromatography and all but **68** were crystallographically characterized. Complex **68**, which includes a formazanate ligand bound to tetrahedral boron in a tridentate fashion is unstable in solution and spontaneously converts to dimers **69** and **71**. Compounds **69** and **70** are structural isomers that differ in the structure of the 10-membered BNCCOBNCCO rings that form their cores (pseudo chair and boat conformations for **69** and **70**, respectively). Each formazanate ligand in complex **69** could be chemically reduced in a stepwise fashion to yield the corresponding radical anion ($\mathbf{69}^{\bullet-}$) and diradical dianion ($\mathbf{69}^{\bullet\bullet 2-}$). BN heterocycles **71** and **72** form by the Lewis-acid-assisted hydrolysis of the nitrile group in the ligand (Scheme 25). Complex **71** spontaneously converts to complex **72** in solution, and the latter can be converted to its corresponding anion ($\mathbf{72}^{-}$) upon reduction with $CoCp_2$ and loss of $H^{\bullet}$.

The optoelectronic properties of BF_2 formazanates have been systematically explored to probe the effect of variation of the R^1, R^3, and R^5 substituents.[61–63,65,69–71] In order to understand trends in these properties, it is vital to first examine the frontier molecular orbitals of BF_2 formazanates as they are directly implicated in their reduction chemistry and low-energy absorption/photoluminescence properties. Fig. 5 shows the HOMO and LUMO isosurfaces calculated using DFT.[64] Both orbitals are

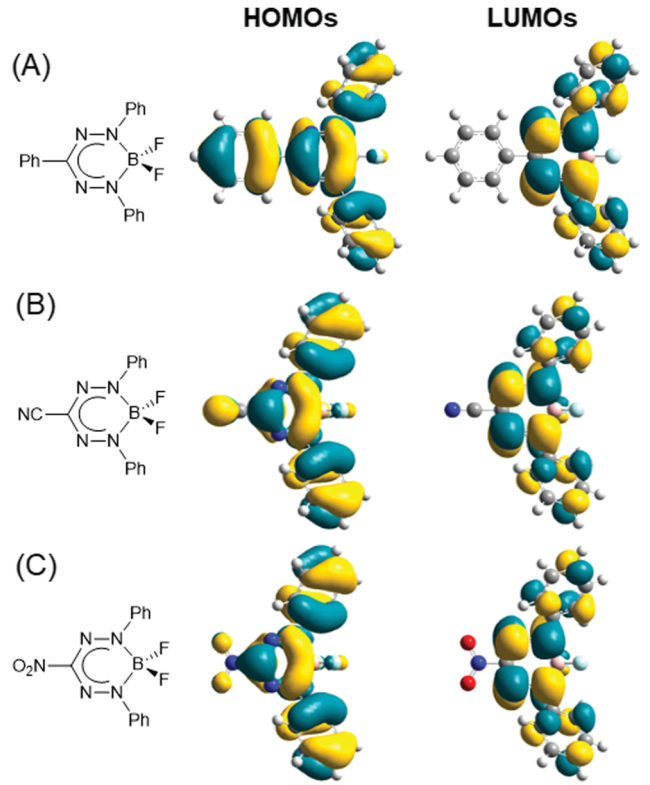

Fig. 5 HOMOs and LUMOs calculated (DFT: M06/6-311+G*) for toluene solutions of BF_2 complexes of (A) triarylformazanate ligands, (B) 3-cyanoformazanate ligands, and (C) 3-nitroformazanate ligands. In all cases Ar^1/Ar^5 = Ph. Adapted from ref. 64 with permission from the American Chemical Society.

highly delocalized over the formazanate backbone and the *N*-aryl substituents for each series of compounds. However, only the HOMOs have significant contribution from the R^3 substituents due to the presence of a nodal plane in the LUMOs. Thus, properties such as electrochemical reduction that implicate only the LUMO are generally affected to a greater extent by structural variation at the *N*-aryl substituents than the R^3 substituents. Properties such as absorption and photoluminescence, which implicate both the HOMO and LUMO (as confirmed by TDDFT[64]) are expected to be affected in a similar fashion, although structural variation at the R^3 substituent cannot be ignored in this context as the HOMOs possess significant contribution from those substituents. Additionally, there is significant orbital density at the *para*-carbons of each aryl ring, indicating that substitution at the *para*-position is likely to have a significant impact on the properties of BF_2 formazanates. General trends have been demonstrated experimentally through systematic studies of BF_2 triarylformazanates.[63]

For brevity, we will discuss the structure–property relationships reported for BF_2 complexes of 3-cyanoformazanate ligands (**60**).[62,64,65,70] Representative data are presented in Fig. 6 and summarized in Table 1. As mentioned above, BF_2 formazanates possess highly delocalized π-electron systems that give rise to low-energy λ_{max} and λ_{PL} values and large Stokes shifts (ν_{ST}). The relative strength of photon absorption can be compared using molar extinction coefficients (ε) while photoluminescence quantum yields (Φ_{PL}) are used to quantify and compare the efficiency of photoluminescence.

Spectroscopic analysis of toluene solutions of **60a** (Ar^1/Ar^5 = Ph) yielded λ_{max} = 502 nm (ε = 30 400 M^{-1} cm^{-1}) and λ_{PL} = 586 nm (Φ_{PL} = 15%) and cyclic voltammetry revealed that this compound can be electrochemically reduced in two one-electron steps at potentials of E_{red1} = −0.53 V and E_{red2} = −1.68 V relative to the $Fc^{0/+}$ redox couple.[62] Coordination of the Lewis acid $B(C_6F_5)_3$ to the nitrogen atom of the 3-cyano substituent in **60a·B(C$_6$F$_5$)$_3$** had little effect on the absorption maxima, although the intensity of the absorption was reduced by approximately one third. While the photoluminescence maximum is unaffected, coordination of $B(C_6F_5)_3$ significantly decreased the quantum yield (Φ_{PL} < 1%) providing an indication that Lewis acid coordination has a substantial effect (*i.e.*, quenching) on the excited state.[65] Increasing the size of the π-electron system by varying the Ar^1/Ar^5 substituents from phenyl to naphthyl in **60b** resulted in a red-shift in λ_{max} by 79 nm (2708 cm^{-1}) and λ_{PL} by 84 nm (2140 cm^{-1}). This extended electronic delocalization also resulted in stabilization of the LUMO orbital, rendering **60b** easier to reduce electrochemically than **60a**.[64] The introduction of *p*-cyanophenyl *N*-aryl substituents in **60c** rendered the complex much easier to reduce than **60a**, as would be expected for an electron-withdrawing substituent. However, perhaps counterintuitively, this structural modification red-shifted the absorption and photoluminescence spectra of **60c** relative to **60a** as a result of the modest increase in the size of the π-electron system when CN groups were introduced.

Complex **60d**, which possesses electron-donating *p*-methoxyphenyl *N*-aryl substituents, yielded absorption and photoluminescence spectra that were dramatically red-shifted and intensified (λ_{max} = 572 nm, ε = 42 700 M^{-1} cm^{-1}; λ_{PL} = 656 nm, Φ_{PL} = 77%) compared to most other BF_2 formazanate complexes (Fig. 6). The dramatic red-shift may be attributed to the donor (*p*-methoxyphenyl) – acceptor (BF_2 formazanate) electronic structure of **60d** and the fact that the oxygen lone pairs can be delocalized into the π-electron system to promote a planar structure. The structural planarity also has implications on the aggregation characteristics of **60d** in THF solutions containing various concentrations of H_2O, where aggregation-caused quenching (ACQ) was observed due to π–π stacking.[71] Detailed studies of the photoexcitation of **60d** revealed that excitation to a high energy, bent excited state with complex vibrational fine structure occurs on the microsecond timescale. This non-emissive state relaxes to the planar, emissive excited state mentioned previously before radiative decay occurs.[72] This behaviour leads to the large Stokes shifts observed for this family of compounds. Complex **60d** was more difficult to reduce to its radical anion and dianion forms when compared to **60a** due to the presence of the electron-donating methoxy substituents. Changing the *N*-aryl substituent from *p*-methoxyphenyl in **60d** to *o*-methoxyphenyl in **60e** resulted in a dramatic change in both the photophysical properties and aggregation behavior due to sterically-driven twisting of the *N*-aryl substituents out of the plane of the BF_2 formazanate ligand. This twisting results in the observation of aggregation-induced

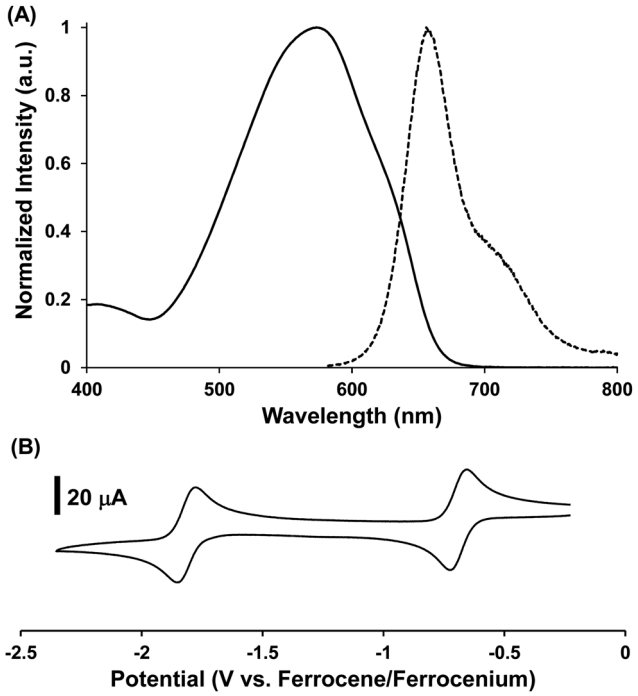

Fig. 6 Representative (A) normalized UV-vis absorption (solid line) and photoluminescence (dashed line) spectra collected in toluene and (B) CV collected at 0.25 V s^{-1} in CH_3CN for **60d**. Adapted from ref. 62 with permission from John Wiley and Sons.

emission enhancement (AIEE) upon the addition of H_2O to THF solutions as the twisted *o*-methoxyphenyl substituents prevent π–π stacking, and thus ACQ.[71] The *m*-substituted complex **60f** had properties intermediate of the *o*- and *p*-derivatives.[70]

Finally, the introduction of strongly electron-donating *p*-dimethylaminophenyl substituents in **60g** resulted in photophysical properties that extend into the near-infrared region of the electromagnetic spectrum and dramatically shifted reduction potentials (λ_{max} = 728 nm, ε = 47 800 M^{-1} cm^{-1}; λ_{PL} = 834 nm, Φ_{PL} = 8%; E_{red1} = −1.02 V and E_{red2} = −2.05 V). Donation of a nitrogen lone pair appears to be the origin of the property changes, and evidence of quinoidal character (*i.e.*, bond alternation within the phenyl ring and N–C bonds with significant double bond character) within the *N*-aryl substituents were observed using X-ray crystallography.[73]

The optoelectronic properties of BF_2 complexes of 3-nitroformazanates (**61**)[64] and triarylformazanates (**59**)[63,65] are qualitatively similar to those described above. The 3-substituent has a dramatic influence on electrochemical reduction potentials with nitroformazanate complexes reduced more easily than analogous compounds based on 3-cyanoformazantes due to the greater electron-withdrawing character of NO_2 relative to CN. The opposite is true for triarylformazante complexes as the C-aryl substituents are relatively weakly electron-withdrawing or electron-donating. The most dramatic difference found within this series is the fact that Φ_{PL} values for BF_2 triarylformazanates are generally very low and often <1% and Stokes shifts for the same species are generally larger than those of 3-cyano and 3-nitro derivatives. The latter trait can be linked to the strictly planar structure adopted by these species in the excited state, as discussed above,[65,74,75] while the former has been attributed to enhanced probability of non-radiative decay associated with vibration and/or free rotation of the 3-aryl substituents. This hypothesis was tested by examining the protonation of compound $\mathbf{59^{Py}}$ to form $\mathbf{59^{Py}{\cdot}H^{+}}$, which possesses a 2-pyridyl substituent at the 3-position of the formazanate backbone.[76] Upon protonation, it is thought that rotation and vibration associated with the 2-pyridyl substituent are dramatically attenuated resulting in enhanced photoluminescence intensity that varied linearly with decreasing pH (Fig. 7).

A second non-radiative decay pathway was uncovered when the Lewis-acid-supported oxoborane (B═O) complex **64** was isolated (Scheme 26).[77] Access to this species required a halide exchange reaction between BF_2 triarylformazanate **59b** (Ar^1/Ar^5 = *p*-tolyl; R^3 = Ph) and BCl_3 to generate BCl_2 complex **63**. The BCl_2 unit in compound **63** was subsequently converted to the oxoborane by treatment with one equivalent of $AlCl_3$ and H_2O. As mentioned earlier, the structural reorganization associated with electronic excitation observed for BF_2 triarylformazanates has been linked to the large Stokes shifts observed for these species. It is also feasible that this structural reorganization is a potential pathway for non-radiative decay upon photoexcitation that contributes to the low Φ_{PL} values observed for this subclass of dyes. The photoluminescence characteristics of oxoborane **64** support this hypothesis, as the formation of the B═O unit turns on photoluminescence (λ_{PL} = 636 nm, Φ_{PL} = 36%).[77] The origin of this behavior lies in the fact that both the ground and excited states of compound **64** adopt a planar structure as the result of sp^2 hybridization at boron, thus limiting structural reorganization upon photoexcitation and attenuating non-radiative decay. Based on these studies, it is reasonable to assume that

Table 1 Optoelectronic properties of BF_2 complexes of 3-cyanoformazanates[62,64,65,70,73]

Compound	Ar^1/Ar^5	$\lambda_{max}{}^a$ (nm)	ε^a (M^{-1} cm^{-1})	$\lambda_{PL}{}^a$ (nm)	$\Phi_{PL}{}^a$ (%)	$\nu_{ST}{}^a$ (nm)	$\nu_{ST}{}^a$ (cm^{-1})	$E_{red1}{}^b$ (V *vs.* $Fc^{0/+}$)	$E_{red2}{}^b$ (V *vs.* $Fc^{0/+}$)
60a	Ph	502	30 400	586	15	84	2855	−0.53	−1.68
60a·B(C_6F_5)$_3$	Ph	502	20 600	632	<1	130	4098	−0.67[c]	−1.75[c]
60b	Naphthyl	581	25 700	670	39	89	2286	−0.49	−1.54
60c	*p*-C_6H_4CN	515	35 000	598	14	83	2695	−0.21	−1.25
60d	*p*-C_6H_4OMe	572	42 700	656	77	84	2239	−0.68	−1.82
60e	*o*-C_6H_4OMe	467	16 000	592	5	125	4521	−0.73	−1.88
60f	*m*-C_6H_4OMe	525	21 100	635	13	110	3300	−0.50	−1.62
60g	*p*-$C_6H_4NMe_2$	728	47 800	834	8	106	1746	−1.02	−2.05

[a] Recorded in toluene. [b] Recorded in CH_3CN. [c] Recorded in dichloroethane.

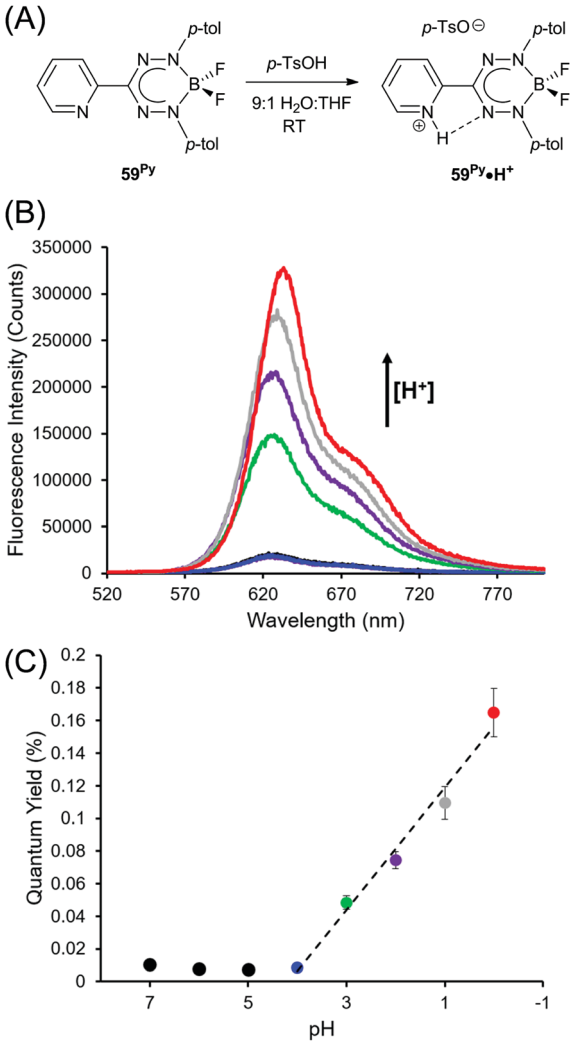

Fig. 7 (A) Protonation of complex **59^{Py}**. (B) pH-Dependent photoluminescence spectra. (C) pH-Dependent photoluminescence quantum yields. Adapted from ref. 76 with permission from the American Chemical Society.

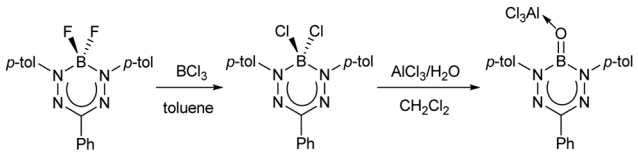

Scheme 26 Synthesis of oxoborane formazanate complex **64**.[77]

maximum photoluminescence from boron triarylformazanate complexes will be achieved with immobilized C-bound substituents and sp^2 hybridized boron units. This remains an area for exploration in the future.

2.8.2 Towards applications: cell imaging, electrochemiluminescence and incorporation in polymeric matrices. Given the extensive use of formazans and related tetrazolium salts **65** (Chart 3) in cell-viability assays,[78] it may not be surprising that BF_2 formazanates have been shown to be biocompatible during their use as cell-imaging agents (Fig. 8).[70,79] BF_2 formazanates

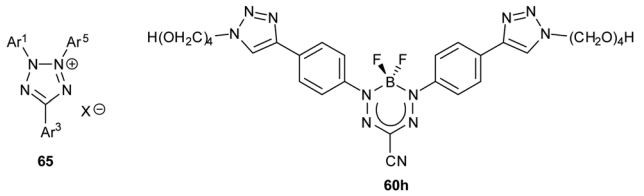

Chart 3

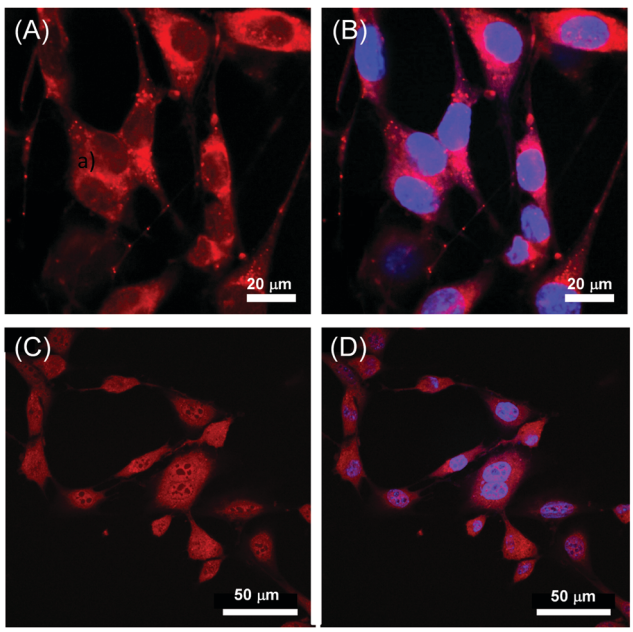

Fig. 8 Confocal fluorescence microscopy images of mouse fibroblast cells with filters applied for the visualization of (A) **60d**, (B) **60d** + DAPI, (C) **60h**, and (D) **60h** + DAPI. Adapted from ref. 70 and 79 with permission from John Wiley and Sons and the Royal Society of Chemistry.

are particularly attractive for this application due to their ready accessibility. Complex **60d** (R^3 = CN, Ar^1/Ar^5 = *p*-methoxyphenyl), was selected for the first study as a result of its relatively high photoluminescence quantum yields in the red region of the electromagnetic spectrum.[70] It is relatively hydrophobic and was therefore introduced into fibroblast cells in DMSO-containing solutions where it accumulated in the hydrophobic cell cytoplasm (Fig. 8A). The simultaneous introduction of 4′,6-diamidino-2-phenylindole (DAPI) allowed for orthogonal imaging of the cell cytoplasm and nucleus when red/blue filters were employed and the resulting images were overlaid (Fig. 8B). The introduction of solubilizing tetraethyleneglycol (TEG) chains at the Ar^1/Ar^5 substituents using copper-assisted azide–alkyne click chemistry (CuAAC) produced **60h** (Chart 3), which was relatively hydrophilic, and drastically changed the cell uptake characteristics of the BF_2 formazanate framework.[79] In the case of **60h**, all features of the fibroblast cells were stained by the complex aside from the DNA-free nucleoli (Fig. 8C) and DMSO was not required for uptake. Once again, in combination with DAPI, **60h** could be used to orthogonally image the cell cytoplasm and nucleus (Fig. 8D). These studies demonstrated the potential impact of structural variation on

the utility of BF_2 formazanates for cell-imaging applications and opened the door for future research in the area. There remains significant opportunity in this area, including the development of imaging agents with improved specificity and disease-targeting capabilities.

Electrogenerated luminescence or electrochemiluminescence (ECL)[80] is a phenomenon that results in the emission of light from an excited state produced by the reaction of electrogenerated species. Ideally, these species will exist at similar oxidation/reduction potentials and are highly reactive. BF_2 formazanates are strong candidates for ECL as a result of their photoluminescence and redox activity. However, it is their oxidation that has proved most useful for the generation of ECL when combined with the coreactant tri-*n*-propylamine (TPrA) (*e.g.*, Fig. 9).[73,75,81]

The CV of a solution containing BF_2 formazanate **60d** and an excess of TPrA is shown in Fig. 9A. Upon scanning to positive potentials, TPrA is first oxidized to its radical cation form ($TPrA^{\bullet+}$), which loses a proton to generate the reducing agent $TPrA^{\bullet}$ (eqn (1)).[82] Fig. 9B shows the intensity of ECL generated during the CV scan as an ECL–voltage curve, and reveals relatively low-intensity ECL centered at *ca.* 1.4 V *vs.* SCE arising from chemical reactions implicating **60d**, $TPrA^{\bullet+}$, and $TPrA^{\bullet}$.[81]

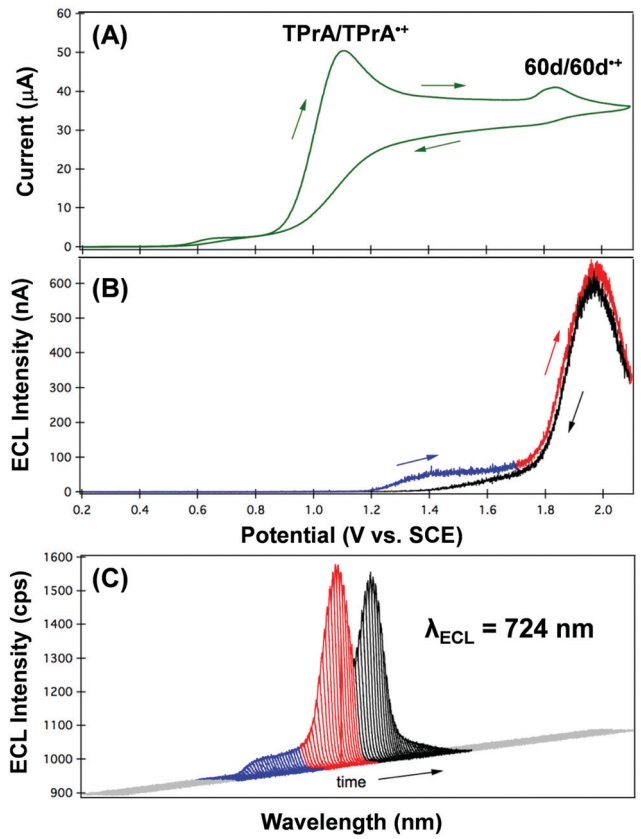

Fig. 9 (A) CV, (B) ECL–voltage curve, and (C) spooling ECL spectra acquired for a 0.1 mM CH_3CN solution of **60d** in the presence of 20 mM TPrA and 0.1 M $[Bu_4N][PF_6]$ at a scan rate of 0.020 V s^{-1}. The wavelength of maximum ECL intensity was 724 nm in all of the spooling ECL spectra reported in panel (C). Adapted from ref. 81 with permission from the Royal Society of Chemistry.

At higher potentials, **60d** is oxidized to $\mathbf{60d}^{\bullet+}$ and $\mathbf{60d}^{2+}$ (eqn (2)) and it was shown computationally that the comproportionation reaction involving $\mathbf{60d}^{2+}$ and **60d** generating two equiv. of $\mathbf{60d}^{\bullet+}$ was energetically favorable (eqn (3)). Thus, the concentration of $\mathbf{60d}^{\bullet+}$ is relatively high above potentials of *ca.* 1.8 V *vs.* SCE. In these potential regions, $\mathbf{60d}^{\bullet+}$ can react with $TPrA^{\bullet}$ to produce the excited state **60d*** (eqn (4)), which radiatively relaxes to its grounds state by ECL with maximum intensity at a wavelength (λ_{ECL}) of 724 nm (eqn (5)). This process shows little dependence on the scan direction (red and blue regions of Fig. 9B), and can be monitored in real time using spooling ECL spectroscopy. Crucially, the spooling spectra (color coded in Fig. 9C) all have ECL maxima centered at 724 nm, indicating a common excited state (**60d***) throughout the entire scan window.

$$\mathrm{TPrA} \xrightarrow{-e^-} \mathrm{TPrA}^{\bullet+} \xrightarrow{-H^+} \mathrm{TPrA}^{\bullet} \quad (1)$$

$$\mathbf{60d} \xrightarrow{-e^-} \mathbf{60d}^{\bullet+} \xrightarrow{-e^-} \mathbf{60d}^{2+} \quad (2)$$

$$\mathbf{60d} + \mathbf{60d}^{2+} \rightarrow 2\,\mathbf{60d}^{\bullet+} \quad (3)$$

$$\mathbf{60d}^{\bullet+} + \mathrm{TPrA}^{\bullet} \rightarrow \mathbf{60d}^{*} + \mathrm{Pr}_2^{\oplus}\mathrm{N}{=}\mathrm{CHCH_2CH_3} \quad (4)$$

$$\mathbf{60d}^{*} \rightarrow \mathbf{60d} + h\nu \quad (5)$$

The ECL efficiency of BF_2 formazanates is dependent on a number of factors, including: match with the oxidation potential of TPrA, the stability/instability of the radical cation and dication forms, and the balance between radiative and non-radiative decay pathways associated with the excited states involved in ECL. The efficiency (Φ_{ECL}) of these processes was quantified by relative comparison with the $[Ru(bipy)_3][PF_6]_2$/TPrA system under identical conditions. Complex **60d** had a maximum ECL efficiency of 450%, which remains the highest reported to date for BF_2 formazanates.[81] The λ_{ECL} and Φ_{ECL} values reported for related compounds are summarized in Table 2.

The attractive optoelectronic properties of BF_2 formazanates make them excellent candidates for incorporation into functional polymers, whereby film-forming properties may facilitate their incorporation into various organic electronics. One of the primary challenges in their polymerization is the discovery of reaction conditions that are compatible with BF_2 formazanates. Ring-opening metathesis polymerization (ROMP)[83] has been used to produce side-chain polymers comprised with pendant BF_2 triarylformazanates **66**[84] and 3-cyanoformazanates **67** (Chart 4).[85] Polymer **66** retained many of the traits of molecular BF_2 triarylformazanates, including intense absorption in the red

Table 2 ECL properties of BF_2 formazanate complexes[73,75,81]

Compound	R^1/R^5	R^3	λ_{ECL} (nm)	Max. Φ_{ECL}[a] (%)
60d	*p*-C_6H_4OMe	CN	724	450
60g	*p*-$C_6H_4NMe_2$	CN	910	18
59c	*p*-C_6H_4OMe	Ph	704	244
59d	*p*-C_6H_4OMe	*p*-C_6H_4OMe	723	94

[a] Relative to the $[Ru(bipy)_3][PF_6]_2$/TPrA benchmark under identical conditions.

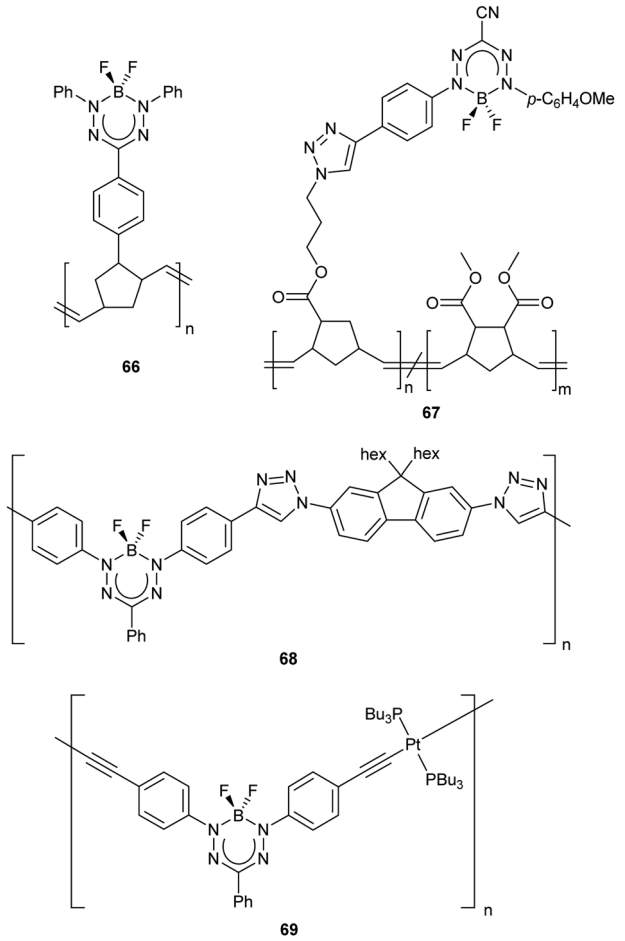

Chart 4

region (λ_{max} = 518 nm), weak photoluminescence (λ_{PL} = 645 nm, Φ_{PL} = 2.5%) and reversible reduction to its poly(radical anion) form (E_{red1} = −0.95 V *vs.* $Fc^{0/+}$).[84] In an effort to enhance photoluminescence intensity, (co)polymers **67** containing BF_2 3-cyanoformazanate complexes were prepared through variation of the mole fraction (f_{BF_2}) of BF_2 formazanate monomer incorporated.[85] Despite the monomer exhibiting respectable photoluminescence (λ_{PL} = 561 nm, Φ_{PL} = 30%), the photoluminescence intensity of solutions of homopolymer **67** (f_{BF_2} = 1) were reduced (λ_{PL} = 559 nm, Φ_{PL} = 11%), likely as a result of ACQ. To circumvent this issue, random (co)polymers with *cis*-dimethyl-5-norbornene-*exo*-2,3-dicarboxylate were produced in order to increase the average distance between the BF_2 formazanates. This strategy resulted in reduced quenching and enhanced photoluminescence up to a maximum of Φ_{PL} = 24% when f_{BF_2} was 0.08. These findings may provide opportunity for side-chain BF_2 formazanate polymers to be used as the active layer in electroluminescent devices in the future.

While side-chain polymers of BF_2 formazanates allow for their desirable characteristics to be combined with advantageous film-forming properties, main-chain polymer architectures offer the latter in combination with opportunities to tune electronic structure *via* extended π-electron conjugation. For example, CuAAC chemistry was used to produce polymer **68** (Chart 4), which gave rise to λ_{max} = 557 nm (ε = 25 700 M^{-1} cm^{-1}) and λ_{PL} = 696 nm (Φ_{PL} = 1%) in DMF.[86] Polymer **68** also exhibited a reversible wave associated with its electrochemical reduction to its poly(radical anion) form (E_{red1} = −0.73 V *vs.* $Fc^{0/+}$). Thorough examination of the properties of **68** compared to model compounds constructed from various combinations of the building blocks of the polymer later revealed that π-electron conjugation involving the BF_2 formazanate units did not extend beyond the triazole rings formed during polymerization. Despite the relatively localized electronic structure, polymer **68** exhibited a narrow thin-film optical band gap (E_g) of 1.7 eV. The combination of BF_2 formazanates and Pt(II) acetylides in polymer **69** (Chart 4) resulted in further narrowing of the band gap (E_g = 1.4 eV), which could be readily tuned *via* the stepwise reduction of the BF_2 formazanate repeating units, providing an entry point for future studies of their redox-tunable semiconductivity.[87] The red-shifted absorption maxima (λ_{max} = 661 nm, ε = 45 500 M^{-1} cm^{-1}) exhibited by polymer **69** relative to its parent BF_2 formazanate unit arises due to extended π-conjugation through the Pt(II) acetylides units that implicates backbonding-type interactions between the π* orbitals of the alkyne units and the d_{xy} and d_{xz} orbitals of the Pt(II) center. The extended electronic conjugation mentioned above was verified by comparison with model compounds constructed from the various polymer building blocks, which in all cases absorbed at shorter wavelengths than polymer **69**. A follow-up study focused on examining the photoluminescence properties of molecular analogues of **69** revealed that conjugation of BF_2 formazanates with Pt(II) acetylides resulted in fluorescence quenching with no signs of phosphorescence observed, even at 77 K.[88]

2.8.3. Boron substituents other than F. The production of boron dihydride (BH_2) complexes of chelating N-donor ligands offers unique opportunities for further reactivity involving the boron-bound hydrides and a representative reaction involving BH_2 formazanates is shown in Scheme 27.[89] The formazan was converted to its corresponding BH_2 complex **70** by treatment with $BH_3{\cdot}SMe_2$ in toluene at room temperature. Heating pure samples of **70** in C_6D_6 resulted in consecutive thermally-induced hydride transfer reactions to yield compounds **71-i/ii** and **72-i/ii**. The observed formation of these isomers provides an indication that hydride transfer can occur at both *N*-aryl substituents in this system, although similar reactivity was not observed for complexes containing *N*-bound C_6F_5 substituents.

The mechanism of these unusual reactions warrants further discussion, and is proposed in Scheme 27b. Step 1 involves the isomerization of complex **70** to form complex **73**, which possesses a 5-member formazanate chelate ring. Similar isomerization behavior has previously been observed for Zn adducts of formazanate ligands.[56] Step 2 involves hydride transfer to the *N*-aryl substituent, exclusively at the *ortho* position, to generate **74**. Step 3 results in hydrogen migration from the cyclohexadiene group to the terminal nitrogen atom, resulting in rearomatization of the *N*-aryl substituent in **71-ii**. Step 4 generates a formally low-valent boron center *via* transfer of the remaining borohydride to the internal nitrogen atom in **75**, which allows

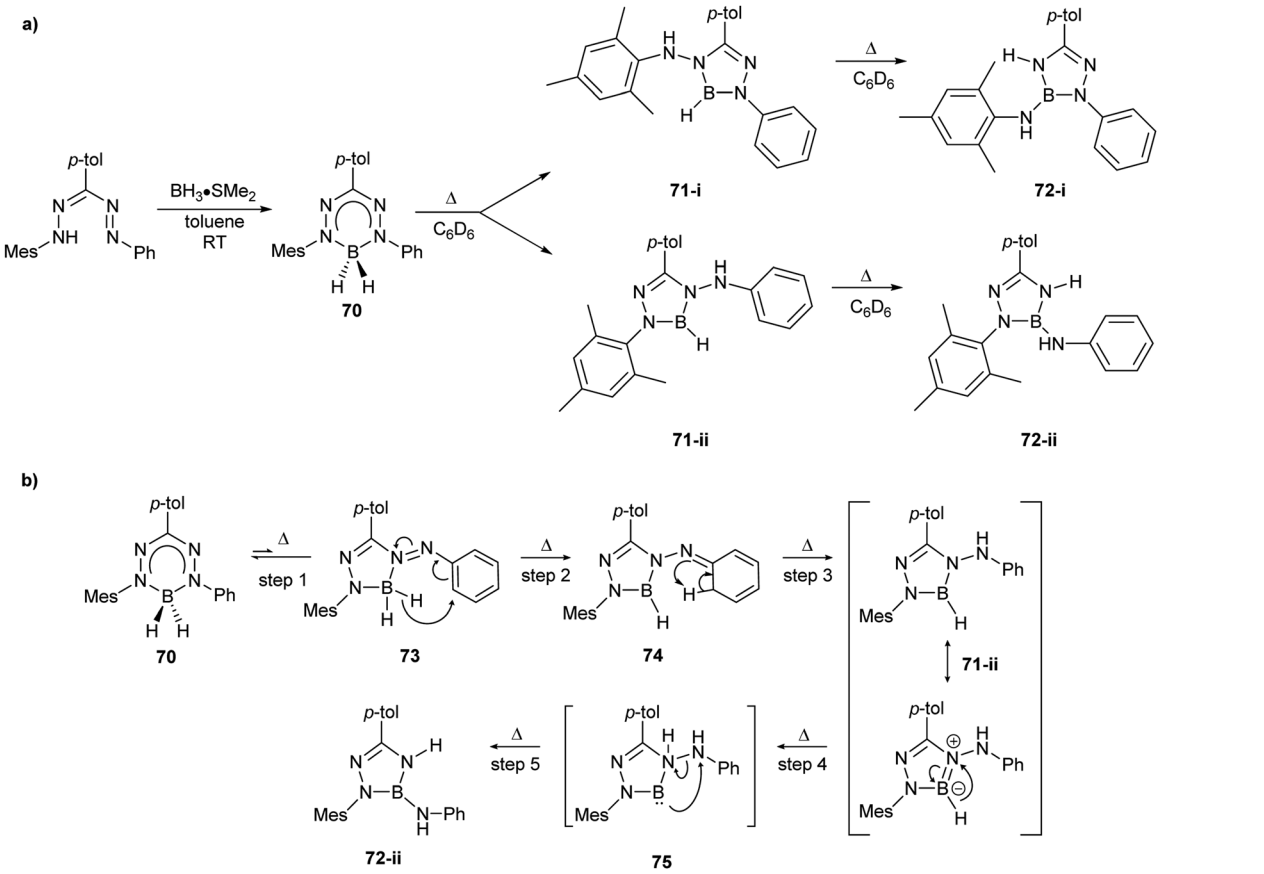

Scheme 27 (a) Representative synthesis of BH_2 formazanate complex **70** and subsequent thermally-driven hydride transfer reactions.[89] (b) Proposed mechanism of thermally-induced hydride transfer reactions of BH_2 formazanate complex **70**.[89]

for reductive N–N bond cleavage to form triamidoborane **71-ii**. DFT calculations (B3LYP/6-31G(d)) indicated that the isomerization step was energetically uphill (5.0 kcal mol^{-1} for **70** → **73**) and that all other steps are energetically downhill.[89] These studies provided significant insight into the use of formazanate ligands as redox-active ligands as each hydride transfer corresponds to the transfer of two electrons and a proton and served as a starting point for further reactivity studies.

As noted earlier (Scheme 24), a significant hurdle in the development of the two-electron reactivity of complexes of redox-active formazanate ligands is the realization of methods for the production of their dianion form. Boron diphenyl (BPh_2) formazanates are excellent candidates for this purpose as the absence of boron–halide bonds in their frameworks should circumvent the formation of salts (*e.g.*, LiF in Scheme 24) that complicated the redox reactivity of BF_2 formazanates.[67] BPh_2 formazanate **76** was generated by refluxing BPh_3 with the appropriate formazan in toluene (Scheme 28a).[90] The radical anion **76**$^{\bullet-}$ and dianion **76**$^{2-}$ were subsequently generated by treatment with 1 equiv. of $CoCp^*_2$ and 2 equiv. of $Na/C_{10}H_8$, respectively. Their solid-state structures were confirmed crystallographically. Crucially, for the first time, the dianion of a formazanate complex was produced, setting the stage for further reactivity studies designed to take advantage of the unique two-electron redox chemistry of the formazanate ligand scaffold.

Reaction of dianion **76**$^{2-}$ with benzyl bromide (BnBr) or H_2O resulted in the production of novel anionic analogues of leucoverdazyls (*e.g.*, **77**) that demonstrated the ability of the formazanate ligand framework to store two electrons and an electrophile (Scheme 28b).[91] The N–Bn or N–H bonds formed were highly reactive, and favored homolytic cleavage pathways due to the inherent stability of the relevant radical anions (*e.g.*, **76**$^{\bullet-}$). This was experimentally demonstrated, for example, by reacting **77** with the (2,2,6,6-tetramethylpiperidin-1-yl)oxyl radical (TEMPO) in THF, resulting in the regeneration of **76**$^{\bullet-}$ and the formation of adduct **78**. This reactivity clearly demonstrated that the unique redox chemistry of formazanate ligands can be used to transfer electrons to electrophiles, in these cases resulting in the formation of Bn$^{\bullet}$ and H$^{\bullet}$.

BF_2 formazanate **59e** was converted to the corresponding dialkynylborane complexes **79** upon treatment with a slight excess of alkynyllithium reagents in yields ranging from 17–35%,[92] which were lower than related dipyrrin complexes[93] as a result of steric crowding imposed by the *N*-aryl substituents (Scheme 29a). These complexes provided an opportunity to study the relationship between structure and properties *via* variation of boron-bound substituents (Table 3). The λ_{max} values obtained for toluene solutions of dialkynylborane complexes **79a–c** were red-shifted by *ca.* 10 nm compared to the parent BF_2 complex **59e** and were relatively insensitive to the nature of the alkyne substituents

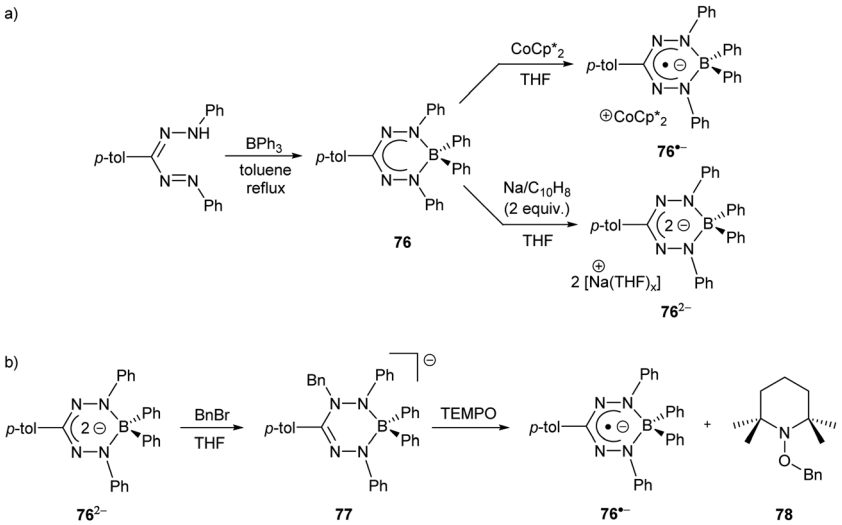

Scheme 28 Representative (a) synthesis and chemical reduction chemistry of BPh_2 formazanate complexes[90] and (b) bond formation/homolysis reactions involving **76**$^{2-}$ and BnBr.[91]

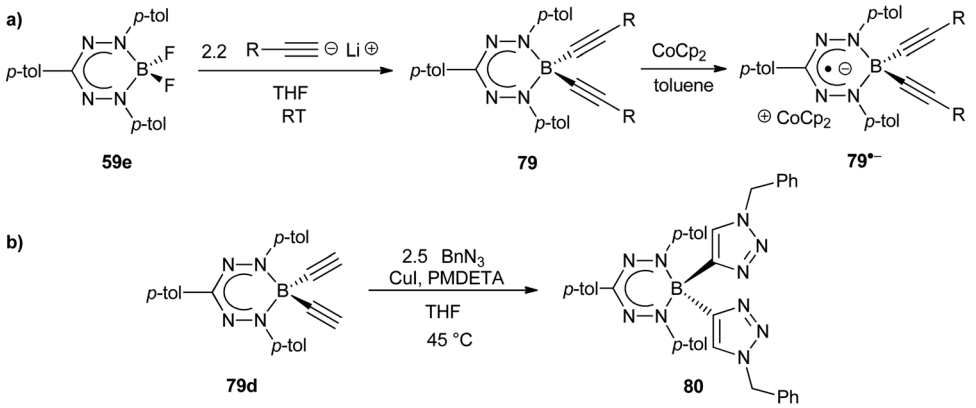

Scheme 29 (a) Synthesis of dialkynylborane formazanate complexes **79**. (b) Proof of concept CuAAC chemistry to produce bis(triazolyl)borane complex **80**.[92]

Table 3 Optoelectronic properties of complexes **59e** and **79a–c**[92]

Compound	R	λ_{max}[a] (nm)	ε[a] (M^{-1} cm^{-1})	E_{red2}[b] (V *vs.* $Fc^{0/+}$)	E_{red1}[b] (V *vs.* $Fc^{0/+}$)	E_{ox1}[b] (V *vs.* $Fc^{0/+}$)
59e	—	532	20 200	−1.99[c]	−1.04	1.03
79a	H	521	12 000	−2.03[c]	−1.18	0.83
79b	OMe	519	12 500	−2.12[c]	−1.21	0.86[d]
79c	CF_3	521	13 700	−2.01[c]	−1.14	0.89

[a] Recorded in toluene. [b] Recorded in CH_2Cl_2. [c] Irreversible peak. Potential at maximum cathodic current reported. [d] Irreversible peak. Potential at maximum anodic current reported.

employed. This insensitivity arises as a result of the tetrahedral geometry at boron, which prevents π-orbital overlap between the formazanate and substituted alkynes. The dialkynylborane complexes could be electrochemically reduced in two steps (**79** → **79**$^{\bullet-}$ and **79**$^{\bullet-}$ → **79**$^{2-}$), and also exhibited reversible oxidation (**79** → **79**$^{\bullet+}$) waves in CH_2Cl_2. The potentials at which these events occurred were dependent on the nature of the alkyne substituents, due to inductive effects, with electron-donating substituents (*e.g.*, **79b**, R = OMe) rendering the complexes easier to oxidize and harder to reduce than the corresponding phenylacetylene complex **79a**. The opposite trend was observed when electron-withdrawing substituents were introduced in complex **79c** (R = CF_3). Chemical reduction with $CoCp_2$ or $CoCp^*_2$ resulted in the formation of stable radical anions (**79**$^{\bullet-}$). Future opportunities in this area should focus on energy/electron transfer between the formazanate ligand backbone and alkynyl substituents bearing π-conjugated functional groups for light-harvesting and charge-transport applications.

Dialkynylborane complexes **79** also provided an opportunity for the elaboration of the structural diversity of boron formazanate complexes using CuAAC chemistry. For example, the reaction of complex **79d** (R = H) with benzyl azide (BnN_3)

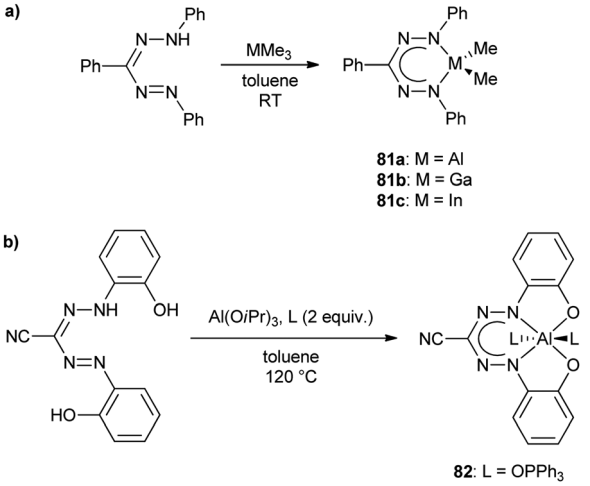

Scheme 30 (a) Synthesis of heavy group 13 complexes of formazanates **81**.[94] (b) Representative synthesis of octahedral aluminum formazanate complexes with phosphine oxide substituents **82**.[95]

resulted in triazole formation at the boron-bound alkyne and demonstrated that, despite the steric congestion at boron, this transformation is feasible and complex **80** could be formed (Scheme 29b). This reactivity could be used to leverage the applications described above or even to produce polymeric structures if bifunctional dialkynylborane formazanate complexes and azides were employed.

2.8.4. Heavier group 13 complexes. In comparison to boron formazanate complexes, heavier group 13 analogues have received relatively little attention. The Sundermeyer group prepared the first heavy group 13 complexes of formazanates **81a–c** by stirring the respective MMe_3 (M = Al, Ga, In) species with a triarylformazan in toluene (Scheme 30a).[94] These complexes contained tetrahedral group 13 atoms and were generally moisture sensitive, although this sensitivity was attenuated by the coordination of dimethylaminophyridine (DMAP) when M = In. Complexes **81a–c** exhibited low-energy absorption maxima and large molar extinction coefficients (**81a:** λ_{max} = 559 nm, ε = 16 210 M^{-1} cm^{-1}; **81b:** λ_{max} = 576 nm, ε = 20 960 M^{-1} cm^{-1}; **81c:** λ_{max} = 591 nm, ε = N/A).[94] Preliminary CV studies indicated that the complexes could not be reversibly oxidized or reduced.

Six-coordinate aluminum complexes of $N_2O_2^{3-}$ formazanate ligands (*e.g.*, **82**) were prepared by heating *N*-(*ortho*-hydroxyphenyl) substituted cyanoformazan with $Al(OiPr)_3$ and two equiv. of phosphine oxide ligand in hot toluene solution resulting in their production in 52–86% yield (Scheme 30b).[95] The solid-state structures of these complexes confirmed an octahedral geometry at aluminum with the formazanate adopting a planar structure and a tetradentate binding mode. DFT calculations (M06/6-311+G(d,p)) indicated that the frontier orbitals were centered on the formazanate ligand, consistent with the fact that variation of the phosphine oxide ligands involved had little effect on the spectroscopic characteristics of the resulting complexes. In the case of complex **82**, its photophysical properties were examined in detail revealing the following data: λ_{max} = 629 nm, ε = 24 700 M^{-1} cm^{-1}; λ_{PL} = 690 nm, Φ_{PL} = 2%. It is worth noting that the low-energy maximum was accompanied by related peaks associated with the vibrational fine structure of the rigid complex (**82**) and that detailed studies of these properties indicated that the phosphine oxide ligands were labile in solution. Examination of the same properties in the presence of 50 equiv. of phosphine oxide ligand confirmed that the emissive species was indeed the octahedral complex **82.** The CV of **82** both in the absence and presence of excess triphenyl phosphine revealed irreversible oxidation and reduction events, with the latter giving rise to the following potentials at peak anodic and cathodic currents: E_{pc} = −1.34 V and E_{pa} = 0.29 V. The combined photoluminescence and oxidation behavior of **82** prompted the examination of its ECL in the presence of TPrA and excess phosphine oxide. These studies gave rise to λ_{ECL} = 735 nm and Φ_{ECL} = 7%, demonstrating for the first time that aluminum formazanate complexes may offer utility in light-emitting technologies.

More recently, Mondol and Otten conducted a study that led to the dramatic expansion of the structural diversity of aluminum formazanate complexes, including the first isolated examples of ligand-supported radical anions and dianions derived from aluminum formazanates.[96] Their work began with the synthesis of tetrahedral AlR_2 complexes (R = Me, Et) that were similar to those reported by Sundermeyer and co-workers.[94] Treatment with one equivalent or excess I_2 resulted in the asymmetrically substituted AlMeI and AlEtI complexes, respectively.

The reaction of potassium salt **9** with $AlCl_3$ in THF yielded a distorted trigonal bipyramidal (τ = 0.64) aluminum formazanate complex **83** (Scheme 31a), which yielded a ^{27}Al NMR resonance at 43.0 ppm. In contrast to most group 13 adducts of formazanate ligands, the low-energy absorption maxima observed for **83** was

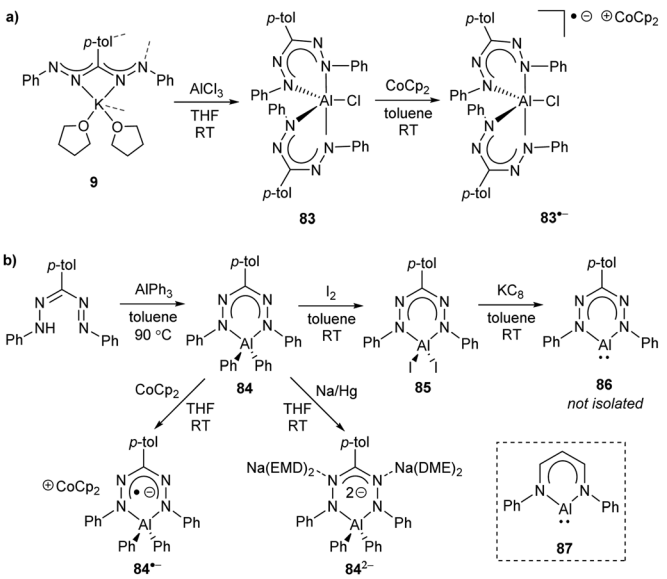

Scheme 31 (a) Synthesis of aluminum formazanate complex **83** and its corresponding radical anion. (b) Synthesis of diphenyl aluminum complex **84** and its conversion to radical anion **84**$^{\bullet-}$, dianion **84**$^{2-}$, and aluminum diodide complex **85**. The attempted conversion of compound **85** to Al(I) carbenoid **86** and the structure of β-diketiminate complex **87** are also included to supplement the discussion above.[96]

blue-shifted by *ca.* 10 nm compared to the parent formazan. This behavior was attributed to a significant structural distortion associated with the Al atom being displaced by more than 1 Å from the plane of the formazanate ligand that causes the ligand backbone to deviate from planarity. Complex **83** exhibited two quasi-reversible reduction waves at potentials of −1.36 V and −1.67 V relative to the $Fc^{0/+}$ redox couple when studied by cyclic voltammetry in THF and was cleanly converted to its radical anion form $\mathbf{83}^{\bullet-}$ by treatment in the same solvent with $CoCp_2$. Density functional calculations indicated that the unpaired electron density associated with this radical anion was primarily located on the nitrogen atoms of both formazanate ligands.

The reaction of triarylformazan with $AlPh_3$ afforded the tetrahedral diphenyl aluminum complex **84** and created several new synthetic opportunities (Scheme 31b). Firstly, isolable radical anion $\mathbf{84}^{\bullet-}$ and dianion $\mathbf{84}^{2-}$ were prepared by treatment with $CoCp_2$ or Na/Hg amalgam, respectively. Ligand exchange resulting from the treatment of complex **84** with I_2 yielded complex **85**. Inspired by the work of Roesky on low-valent Al chemistry supported by β-diketiminate ligands,[97] complex **85** was treated with two equiv. of KC_8 with the goal of performing a two-electron reduction. The observed color changes were indicative of radical anion formation, but the Al(I) carbenoid **86** was not isolated from this reaction. This prompted a detailed investigation of the electronic structures of proposed complex **86** and the related β-diketiminate complex **87** using DFT calculations. As expected, the presence of additional nitrogen atoms in the ligand backbone of **86** resulted in the stabilization of the HOMO, LUMO, and LUMO+1 orbitals relative to those of **87** (Table 4). However, this did not explain the apparent difference in stability between the two families of compounds. Examination of the singlet–triplet energy gaps for each species provided further insight. The calculated values were 11.5 kcal mol^{-1} for the formazanate complex **86** and 30.7 kcal mol^{-1} for β-diketiminate complex **87**, with the marked difference potentially accounting for the differences in observed reactivity.

Comparison of structure, bonding, and reactivity of $AlPh_2$ complex $\mathbf{84}^{2-}$ with its BPh_2 analogue $\mathbf{76}^{2-}$, both possessing formazanate ligands in their trianionic form, led to several important conclusions.[98] (i) The Al–N bonds have primarily ionic character and B–N bonds have primarily covalent character. (ii) The introduction of an Al ion resulted in N–C_{aryl} bonds with significant π character; a structural feature that appears to have been recently exploited to induce near-IR absorption and emission in similar compounds.[73] (iii) Coordination of Al significantly alters the reactivity at the unsubstituted nitrogen atoms, weakening the N–Bn bonds in trapped species (*e.g.*, 77) and setting the stage for two-electron redox chemistry to be exploited.

Table 4 Calculated frontier orbital energies and single-triplet energy gaps for low-valent aluminum complexes with formazanate and β-diketiminate ligands at the B3LYP/6-311G(d,p) level of theory. Reproduced from ref. 96 (https://pubs.acs.org/doi/10.1021/acs.inorgchem.9b00553) with permission from the American Chemical Society. Further permissions related to the material excerpted should be directed to the ACS

$-(E_S - E_T)$ (kcal mol^{-1})	HOMO (eV)	LUMO (eV)	LUMO+1 (eV)
11.5	−5.25	−3.00	−1.43
30.7	−4.77	−1.79	−0.80

2.9 Group 14 (Si, Ge, Sn)

The first examples of group 14 formazanate complexes were reported in 2018.[99] After deprotonating 1,5-bis(2-hydroxyphenyl)-3-phenylformazan with NaH to generate its trianion, the formazanate was combined with the respective phenyl trichloride of Si, Ge, and Sn ($EPhCl_3$) in THF to form complexes **88a–c** (Scheme 32), which contain hypervalent (5-coordinate) group 14 atoms. Unlike closely related hypervalent group 14 complexes of dipyrrin $N_2O_2^{3-}$ ligands that adopted a trigonal bipyramidal geometry,[100] **88a–c** adopt a distorted square pyramidal geometry. This is particularly relevant when considering the potential conversion of these complexes to their corresponding radical anions $\mathbf{88a–c}^{\bullet-}$, where π-electron delocalization is required to enhance radical stability. The formazanate ligand occupies the base of the distorted square pyramid formed by the respective ligands, imparting planarity. This planar configuration led to a delocalized structure and low-energy absorption maxima of 662 nm (ε = 16 800 M^{-1} cm^{-1}) for **88a**, 681 nm (ε = 21 200 M^{-1} cm^{-1}) for **88b**, and 681 nm (ε = 22 200 M^{-1} cm^{-1}) for **88c** in CH_2Cl_2 (Fig. 10A–C), and varied

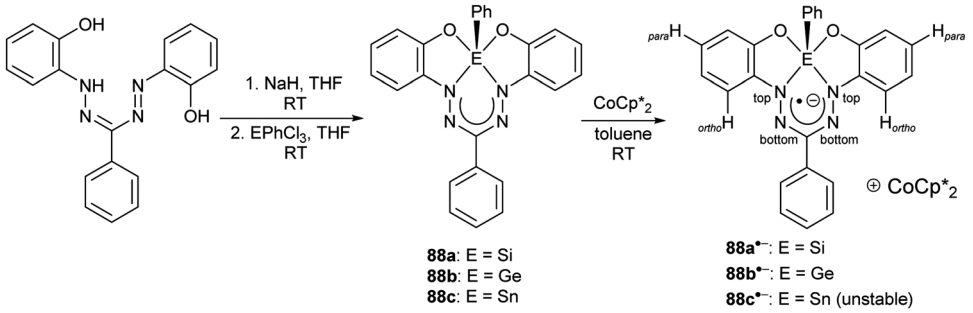

Scheme 32 Synthesis of group 14 complexes of formazanate ligands **88a–c** and their corresponding radical anions $\mathbf{88a–c}^{\bullet-}$.[99]

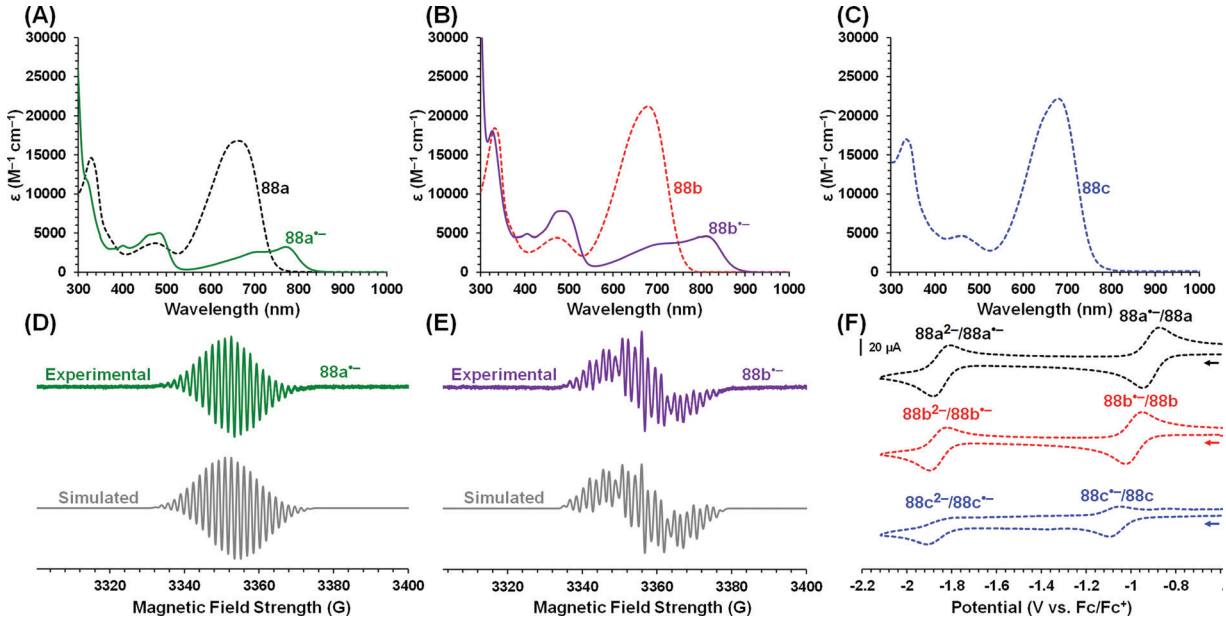

Fig. 10 (A–C) UV-vis absorption spectra of complexes **88a–c** and radicals **88a**$^{\bullet-}$ and **88b**$^{\bullet-}$, (D and E) EPR spectra of radicals **88a**$^{\bullet-}$ and **88b**$^{\bullet-}$, and (F) CVs of complexes **88a–c** (0.25 V s^{-1}) recorded in dry, degassed CH_2Cl_2 containing *ca.* 1 mM analyte and 0.1 M $[Bu_4N][PF_6]$. The arrows denote the scan direction.[99] Reproduced from ref. 99 with permission from John Wiley and Sons.

based on the group 14 element incorporated. The planarity of the formazanate ligand was quantified by assessing the displacement of the group 14 atom from the N_4O_2 plane (**88a**: 0.467 Å; **88b**: 0.593 Å; **88c**: 0.739 Å) and the average angle between the N_4O_2 plane and the plane defined by the *N*-aryl substituents (**88a**: 22.44°; **88b**: 22.63°; **88c**: 26.81°) in the solid state. When the relatively large Sn atom was incorporated in **88c**, the solid-state structure deviated from planarity significantly. This influenced the electronic properties of the resulting complex, and rendered **88c** more difficult to reduce than **88a** and **88b** as a result of a destabilized LUMO orbital that results from disruption of the π-electron system. Furthermore, the reduction events associated with radical anion and dianion formation that were reversible in the CVs collected for **88a** and **88b** became irreversible for **88c** (Fig. 10F). This was reflected during efforts to chemically reduce **88a–c** to **88a–c**$^{\bullet-}$, with the Sn-containing compound **88c**$^{\bullet-}$ being the only unstable compound in the series as a result of the poorer electron-accepting ability of its relatively less planar formazanate ligand. Radicals **88a**$^{\bullet-}$ and **88b**$^{\bullet-}$ were structurally characterized, once again revealing square pyramidal geometries at Si and Ge, reduced separation between the main group atoms and the N_4O_2 plane, and an overall greater degree of formazanate ligand planarity. In solution, these species gave rise to new absorption bands centered at *ca.* 800 nm (consistent with verdazyl-type radicals) and complex EPR spectra implicating hyperfine coupling to the *ortho*- and *para*-protons of the *N*-aryl substituents and two sets of equivalent nitrogen atoms of the formazanate backbone. Simulation of the spectra, yielded the following *g*-factors and hyperfine coupling constants (*a*) for **88a**$^{\bullet-}$: g = 2.0037, $a_{N(bottom)}$ = 5.05 G, $a_{N(top)}$ = 3.37 G, $a_{H(ortho)}$ = 1.61 G, $a_{H(para)}$ = 1.58 G and **88b**$^{\bullet-}$: g = 2.0035, $a_{N(bottom)}$ = 4.94 G, $a_{N(top)}$ = 3.75 G, $a_{H(ortho)}$ = 1.56 G, $a_{H(para)}$ = 1.55 G (Fig. 10D and E). These stable radicals are rare examples that do not require the presence of significant steric bulk as a stabilizing factor and demonstrate the importance of structural planarity and π-electron delocalization for the stabilization of radical species.

2.10 Group 15 (P)

To the best of our knowledge, there have been no reports of compounds prepared by the direct coordination of formazanate ligands to group 15 atoms. However, the Hicks group has reported the synthesis of several examples of phosphaverdazyl radicals *via* indirect routes (Scheme 33).[101–103] Bis(hydrazide)s **89a–c** were reacted with trimethyl orthobenzoate to form phosphaleucoverdazyls **90a–c**. Like their purely organic analogs, the leucoverdazyls were readily oxidized to their radical forms by treatment with NaH/$[Bu_4N][IO_4]$ or benzoquinone to form phosphaverdazyls **91a**$^{\bullet}$**–91c**$^{\bullet}$. These compounds are effectively phosphorus(v) adducts of the radical dianion form of formazanate ligands.

EPR spectroscopic analysis of **91a**$^{\bullet}$ revealed hyperfine coupling constants to two pairs of equivalent nitrogen atoms that were typical of other verdazyl radicals. However, perhaps surprisingly given the non-planar structure of the heterocyclic core, an appreciable hyperfine constant attributed to phosphorus (a_P = 5.2 G) was observed, presumably as a result of spin leakage *via* spin polarization. This observation prompted the study of phosphaverdazyl **91b**$^{\bullet}$, which possesses an additional p orbital on the Me_2N group that could allow for a spiroconjugation pathway for radical transfer from the π-system of the phosphaverdazyl core to the Me_2N group. EPR analysis again revealed typical coupling to two pairs of equivalent nitrogen atoms and an appreciable hyperfine coupling to the exocyclic nitrogen of 4.6 G. To further probe this effect,

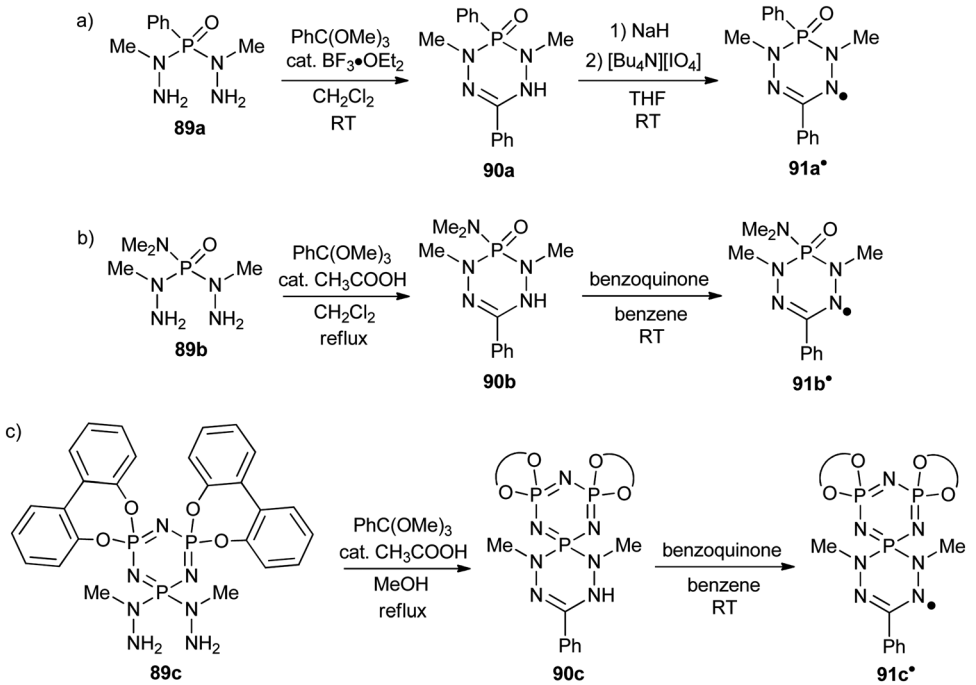

Scheme 33 Synthesis of phosphaverdazyls **91a•–91c•**.[101–103]

phosphaverdazyl **91c•** was prepared and potential radical transfer between the phosphaverdazyl and phosphazene ring was examined. Hyperfine coupling constants <1 G were obtained for the phosphazene nitrogen atoms, indicating inefficient radical transfer despite the seemingly ideal orbital arrangement for electronic communication *via* spiroconjugation of the heterocycle π-systems. The authors therefore concluded that the most likely coupling pathway involved spin polarization through the σ bond framework of the molecules.

3. Conclusions

Formazans (organic compounds with the Ar^1-NH-N=CR^3-N=N-Ar^5 structure) have a venerable history in chemistry, with the development of synthetic procedures dating back to the end of the 1800s. Deprotonation gives rise to monoanionic chelating N-donor ligands ('formazanates') that are related to the well-known β-diketiminate and dipyrrinate classes of ligands, but with distinct electronic features. From the studies of the last two decades discussed in this review it is clear that the relatively straightforward, modular synthesis of the parent formazans allows a facile entry into formazanate complexes with tunable steric/electronic properties. Coordination compounds with formazanate ligands are now known in both the main group as well as d-block of the periodic table. Despite the advances made in recent years, the overview presented here also clearly demonstrates that formazanate complexes of the most electropositive elements (*e.g.*, early transition metals and lanthanides) have not yet been reported. Thus, substantial gaps remain in our understanding of the fundamental coordination chemistry of these ligands, which means that this research area is still very much amenable to further growth.

A feature of formazanate ligands that sets these apart from β-diketiminates/dipyrrinates and other bidentate N-donor ligands is the presence of a delocalized, low-lying LUMO, which is π-anti-bonding between the four nitrogen atoms in the ligand backbone. Complexes with a coordinated formazanate ligand thus generally have a small HOMO–LUMO gap, which results in the intense coloration of these compounds due to symmetry-allowed ($\pi \rightarrow \pi^*$) electronic transitions in the visible range. Moreover, the energetically accessible π*-orbital renders formazanate complexes redox-active, and allows reversible ligand-based storage of electrons in these compounds. In transition metal formazanate complexes, the interaction of the d-orbitals with the close-lying ligand π*-orbital has been shown to lead a high degree of metal–ligand bond covalency (π-backdonation) and unusual electronic/magnetic properties (*e.g.*, spin-crossover, valence tautomerism). With the vast majority of studies on transition metal formazanate compounds focussing on synthetic aspects, not much is known yet on leveraging the distinctive structural, magnetic and spectral properties of these compounds in applications. The same holds true for the reactivity of transition metal formazanate complexes, and the use of formazanates as supporting ligands in organometallic chemistry and homogeneous catalysis is currently little explored. Nevertheless, it is clear that the incorporation of redox-active formazanate ligands leads to reactivity that does not simply mirror that of complexes with related (redox-inert) anionic bidentate N-donor ligands: the possibility to access reduced and/or oxidized states of the formazanate ligand enables new modes of reactivity. An additional aspect that requires further study is the ability of formazanates to access different coordination modes, which potentially allows complexes with these ligands to adapt the coordination sphere around the central element in response to

varying steric/electronic demands throughout a sequence of (catalytic) reaction steps.

Perhaps the most well-established area of application is based on the optoelectronic properties of boron difluoride adducts of the formazanate anion. The absorption and emission spectra of these dyes can be rationally tuned by substituent effects at the formazanate N-Ar[1/5] positions, in particular *via* the extent of π-conjugation. Boron difluoride compounds containing 3-cyano-formazanate ligands combine high photoluminescence quantum yields with large Stokes shifts that render them effective cell-imaging agents. This class of compounds was also used for efficient electrochemiluminescence at potentials >1.8 V *vs.* SCE in the presence of tri-*n*-propylamine. The high stability of formazanate boron compounds bodes well for applications in materials, especially considering that incorporation of redox-active formazanate units in polymers leads to a low band-gap that may be further modified by (partial) reduction.

Studies related to the reduction chemistry of boron and aluminum complexes with formazanate ligands have provided detailed insight in the structure/reactivity of these compounds, demonstrating that ligand-based 'storage' of up to two electrons in a single formazanate ligand is feasible and allows the development of (stoichiometric) multi-electron chemical transformations that are purely ligand-based. In the course of these studies, decomposition pathways have been identified that indicate that cleavage of an N–N bond in the backbone is potentially deleterious.

The parallels that exist between the chemistry of formazanate coordination complexes and that of stable organic verdazyl radicals is perhaps most clearly demonstrated with the recent synthesis of Si, Ge and Sn compounds with a tetradentate formazanate-based N_2O_2 ligand: hypervalent heavier group 14 analogues of verdazyl radicals were obtained that are exceptionally stable despite the absence of sterically demanding substituents or other stabilizing effects.

To conclude, we believe that the fundamental insight that has been accumulated over the last two decades on the synthesis, properties and reactivity of formazanate coordination complexes provides a solid basis for the development of new applications that make use of the distinctive optoelectronic features and versatile electrochemistry that formazanate ligands offer.

Conflicts of interest

There are no conflicts to declare.

Acknowledgements

We would like to thank the University of Western Ontario and the University of Groningen for financial support. Our own work in this area is supported by funding from the NSERC of Canada, the Canadian Foundation for Innovation, the Ontario Ministry of Research and Innovation (JBG) and the Netherlands Organisation for Scientific Research (NWO) *via* VENI and VIDI grants (EO). We also thank Dr. Ryan R. Maar and Francesca Milocco for valuable discussions and proofreading the document.

Notes and references

1 A. W. Nineham, *Chem. Rev.*, 1955, **55**, 355–483.
2 A. S. Shawali and N. A. Samy, *J. Adv. Res.*, 2015, **6**, 241–254.
3 G. N. Lipunova, T. G. Fedorchenko and O. N. Chupakhin, *Russ. J. Gen. Chem.*, 2019, **89**, 1225–1245.
4 E. Grela, J. Kozlowska and A. Grabowiecka, *Acta Histochem.*, 2018, **120**, 303–311.
5 J. C. Stockert, R. W. Horobin, L. L. Colombo and A. Blázquez-Castro, *Acta Histochem.*, 2018, **120**, 159–167.
6 B. D. Koivisto and R. G. Hicks, *Coord. Chem. Rev.*, 2005, **249**, 2612–2630.
7 R. G. Hicks, *Org. Biomol. Chem.*, 2007, **5**, 1321–1338.
8 D. J. R. Brook, *Comments Inorg. Chem.*, 2015, **35**, 1–17.
9 A. R. Katritzky, S. A. Belyakov, D. Cheng and H. D. Durst, *Synthesis*, 1995, 577–581.
10 E. Bamberger and J. Müller, *Ber. Dtsch. Chem. Ges.*, 1894, **27**, 147–155.
11 E. Wedekind, *Ber. Dtsch. Chem. Ges.*, 1897, **30**, 2993–2999.
12 F. A. Neugebauer and H. Trischmann, *Justus Liebigs Ann. Chem.*, 1967, **706**, 107–111.
13 Y. A. Ibrahim, A. H. M. Elwahy and A. A. Abbas, *Tetrahedron*, 1994, **50**, 11489–11498.
14 J. B. Gilroy, P. O. Otieno, M. J. Ferguson, R. McDonald and R. G. Hicks, *Inorg. Chem.*, 2008, **47**, 1279–1286.
15 D. M. Hubbard and E. W. Scott, *J. Am. Chem. Soc.*, 1943, **65**, 2390–2393.
16 L. Bourget-Merle, M. F. Lappert and J. R. Severn, *Chem. Rev.*, 2002, **102**, 3031–3065.
17 R. L. Webster, *Dalton Trans.*, 2017, **46**, 4483–4498.
18 G. I. Sigeikin, G. N. Lipunova and I. G. Pervova, *Russ. Chem. Rev.*, 2006, **75**, 885–900.
19 V. Lyaskovskyy and B. de Bruin, *ACS Catal.*, 2012, **2**, 270–279.
20 O. R. Luca and R. H. Crabtree, *Chem. Soc. Rev.*, 2013, **42**, 1440–1459.
21 B. de Bruin, P. Gualco and N. D. Paul, in *Ligand Design in Metal Chemistry*, ed. M. Stradiotto and R. J. Lundgren, Wiley, 2016, ch. 7, pp. 176–204.
22 R. Travieso-Puente, M.-C. Chang and E. Otten, *Dalton Trans.*, 2014, **43**, 18035–18041.
23 R. Travieso-Puente, S. Budzak, J. Chen, P. Stacko, J. T. B. H. Jastrzebski, D. Jacquemin and E. Otten, *J. Am. Chem. Soc.*, 2017, **139**, 3328–3331.
24 D. A. Brown, H. Bögge, G. N. Lipunova, A. Müller, W. Plass and K. G. Walsh, *Inorg. Chim. Acta*, 1998, **280**, 30–38.
25 A. Müller, H. Bögge, E. Diemann, D. Brown, S. O'Shea and G. Lipunova, *Naturwissenschaften*, 1994, **81**, 136–137.
26 Y. A. Gorbatenko, Z. G. Rezinskikh, G. N. Lipunova, I. G. Pervova, T. I. Maslakova, P. A. Slepukhin and I. N. Lipunov, *Russ. J. Appl. Chem.*, 2008, **81**, 2127–2131.
27 J. B. Gilroy, B. O. Patrick, R. McDonald and R. G. Hicks, *Inorg. Chem.*, 2008, **47**, 1287–1294.
28 R. Travieso-Puente, J. O. P. Broekman, M.-C. Chang, S. Demeshko, F. Meyer and E. Otten, *J. Am. Chem. Soc.*, 2016, **138**, 5503–5506.

29 R. Hoffmann, S. Alvarez, C. Mealli, A. Falceto, T. J. Cahill, T. Zeng and G. Manca, *Chem. Rev.*, 2016, **116**, 8173–8192.
30 D. L. J. Broere, B. Q. Mercado, J. T. Lukens, A. C. Vilbert, G. Banerjee, H. M. C. Lant, S. H. Lee, E. Bill, S. Sproules, K. M. Lancaster and P. L. Holland, *Chem. – Eur. J.*, 2018, **24**, 9417–9425.
31 D. L. J. Broere, B. Q. Mercado, E. Bill, K. M. Lancaster, S. Sproules and P. L. Holland, *Inorg. Chem.*, 2018, **57**, 9580–9591.
32 D. L. J. Broere, B. Q. Mercado and P. L. Holland, *Angew. Chem., Int. Ed.*, 2018, **57**, 6507–6511.
33 F. Milocco, S. Demeshko, F. Meyer and E. Otten, *Dalton Trans.*, 2018, **47**, 8817–8823.
34 A. J. Kamphuis, F. Milocco, L. Koiter, P. P. Pescarmona and E. Otten, *ChemSusChem*, 2019, **12**, 3635–3641.
35 G. B. Jameson, A. Muster, S. D. Robinson, J. N. Wingfield and J. A. Ibers, *Inorg. Chem.*, 1981, **20**, 2448–2456.
36 A. Mandal, B. Schwederski, J. Fiedler, W. Kaim and G. K. Lahiri, *Inorg. Chem.*, 2015, **54**, 8126–8135.
37 N. A. Protasenko, A. I. Poddel'sky, A. S. Bogomyakov, G. K. Fukin and V. K. Cherkasov, *Inorg. Chem.*, 2015, **54**, 6078–6080.
38 N. A. Protasenko, A. I. Poddel'sky, A. S. Bogomyakov, A. G. Starikov, I. V. Smolyaninov, N. T. Berberova, G. K. Fukin and V. K. Cherkasov, *Inorg. Chim. Acta*, 2019, **489**, 1–7.
39 E. Kabir, G. Mu, D. A. Momtaz, N. A. Bryce and T. S. Teets, *Inorg. Chem.*, 2019, **58**, 11677–11683.
40 N. A. Frolova, S. Z. Vatsadze, V. E. Zavodnik, R. D. Rakhimov and N. V. Zyk, *Russ. Chem. Bull.*, 2006, **55**, 1810–1818.
41 L. Hunter and C. B. Roberts, *J. Chem. Soc.*, 1941, 823–826.
42 D. Dale, *J. Chem. Soc. A*, 1967, 278–287.
43 H. Tezcan, E. Uzluk and M. L. Aksu, *Electrochim. Acta*, 2008, **53**, 5597–5607.
44 A. V. Zaidman, I. G. Pervova, A. I. Vilms, G. P. Belov, R. R. Kayumov, P. A. Slepukhin and I. N. Lipunov, *Inorg. Chim. Acta*, 2011, **367**, 29–34.
45 J. B. Gilroy, M. J. Ferguson, R. McDonald and R. G. Hicks, *Inorg. Chim. Acta*, 2008, **361**, 3388–3393.
46 G. N. Lipunova, Z. G. Rezinskikh, T. I. Maslakova, P. A. Slepukhin, I. G. Pervova, I. N. Lipunov and G. I. Sigeikin, *Russ. J. Coord. Chem.*, 2009, **35**, 215–221.
47 F. Milocco, F. de Vries, A. Dall'Anese, V. Rosar, E. Zangrando, E. Otten and B. Milani, *Dalton Trans.*, 2018, **47**, 14445–14451.
48 A. R. Siedle and L. H. Pignolet, *Inorg. Chem.*, 1980, **19**, 2052–2056.
49 E. Kabir, C.-H. Wu, J. I. C. Wu and T. S. Teets, *Inorg. Chem.*, 2016, **55**, 956–963.
50 E. Kabir, D. Patel, K. Clark and T. S. Teets, *Inorg. Chem.*, 2018, **57**, 10906–10917.
51 G. Mu, L. Cong, Z. Wen, J. I. C. Wu, K. M. Kadish and T. S. Teets, *Inorg. Chem.*, 2018, **57**, 9468–9477.
52 S. Hong, L. M. R. Hill, A. K. Gupta, B. D. Naab, J. B. Gilroy, R. G. Hicks, C. J. Cramer and W. B. Tolman, *Inorg. Chem.*, 2009, **48**, 4514–4523.
53 S. J. Hong, A. K. Gupta and W. B. Tolman, *Inorg. Chem.*, 2009, **48**, 6323–6325.
54 R. M. Rush and J. H. Yoe, *Anal. Chem.*, 1954, **26**, 1345–1347.
55 M.-C. Chang, T. Dann, D. P. Day, M. Lutz, G. G. Wildgoose and E. Otten, *Angew. Chem., Int. Ed.*, 2014, **53**, 4118–4122.
56 M.-C. Chang, P. Roewen, R. Travieso-Puente, M. Lutz and E. Otten, *Inorg. Chem.*, 2015, **54**, 379–388.
57 J. B. Gilroy, M. J. Ferguson, R. McDonald, B. O. Patrick and R. G. Hicks, *Chem. Commun.*, 2007, 126–128.
58 D. Frath, J. Massue, G. Ulrich and R. Ziessel, *Angew. Chem., Int. Ed.*, 2014, **53**, 2290–2310.
59 A. Loudet and K. Burgess, *Chem. Rev.*, 2007, **107**, 4891–4932.
60 Y. Ni and J. Wu, *Org. Biomol. Chem.*, 2014, **12**, 3774–3791.
61 M.-C. Chang and E. Otten, *Chem. Commun.*, 2014, **50**, 7431–7433.
62 S. M. Barbon, P. A. Reinkeluers, J. T. Price, V. N. Staroverov and J. B. Gilroy, *Chem. – Eur. J.*, 2014, **20**, 11340–11344.
63 S. M. Barbon, J. T. Price, P. A. Reinkeluers and J. B. Gilroy, *Inorg. Chem.*, 2014, **53**, 10585–10593.
64 S. M. Barbon, V. N. Staroverov and J. B. Gilroy, *J. Org. Chem.*, 2015, **80**, 5226–5235.
65 M.-C. Chang, A. Chantzis, D. Jacquemin and E. Otten, *Dalton Trans.*, 2016, **45**, 9477–9484.
66 N. G. Connelly and W. E. Geiger, *Chem. Rev.*, 1996, **96**, 877–910.
67 M.-C. Chang and E. Otten, *Inorg. Chem.*, 2015, **54**, 8656–8664.
68 S. M. Barbon, V. N. Staroverov and J. B. Gilroy, *Angew. Chem., Int. Ed.*, 2017, **56**, 8173–8177.
69 S. M. Barbon, J. T. Price, U. Yogarajah and J. B. Gilroy, *RSC Adv.*, 2015, **5**, 56316–56324.
70 R. R. Maar, S. M. Barbon, N. Sharma, H. Groom, L. G. Luyt and J. B. Gilroy, *Chem. – Eur. J.*, 2015, **21**, 15589–15599.
71 R. R. Maar and J. B. Gilroy, *J. Mater. Chem. C*, 2016, **4**, 6478–6482.
72 A. Melenbacher, J. S. Dhindsa, J. B. Gilroy and M. J. Stillman, *Angew. Chem., Int. Ed.*, 2019, **58**, 15339–15343.
73 R. R. Maar, R. Zhang, D. G. Stephens, Z. Ding and J. B. Gilroy, *Angew. Chem., Int. Ed.*, 2019, **58**, 1052–1056.
74 A. D. Laurent, E. Otten, B. Le Guennic and D. Jacquemin, *J. Mol. Model.*, 2016, **22**, 263.
75 M. Hesari, S. M. Barbon, R. B. Mendes, V. N. Staroverov, Z. Ding and J. B. Gilroy, *J. Phys. Chem. C*, 2018, **122**, 1258–1266.
76 S. M. Barbon, J. V. Buddingh, R. R. Maar and J. B. Gilroy, *Inorg. Chem.*, 2017, **56**, 12003–12011.
77 R. R. Maar, N. A. Hoffman, V. N. Staroverov and J. B. Gilroy, *Chem. – Eur. J.*, 2019, **25**, 11015–11019.
78 M. V. Berridge, P. M. Herst and A. S. Tan, *Biotechnol. Annu. Rev.*, 2005, **11**, 127–152.
79 S. M. Barbon, S. Novoa, D. Bender, H. Groom, L. G. Luyt and J. B. Gilroy, *Org. Chem. Front.*, 2017, **4**, 178–190.
80 A. J. Bard, *Electrogenerated Chemiluminescence*, Marcel Dekker Inc., 2004.
81 M. Hesari, S. M. Barbon, V. N. Staroverov, Z. F. Ding and J. B. Gilroy, *Chem. Commun.*, 2015, **51**, 3766–3769.
82 R. Y. Lai and A. J. Bard, *J. Phys. Chem. A*, 2003, **107**, 3335–3340.
83 C. W. Bielawski and R. H. Grubbs, *Prog. Polym. Sci.*, 2007, **32**, 1–29.

84 S. Novoa, J. A. Paquette, S. M. Barbon, R. R. Maar and J. B. Gilroy, *J. Mater. Chem. C*, 2016, **4**, 3987–3994.
85 S. Novoa and J. B. Gilroy, *Polym. Chem.*, 2017, **8**, 5388–5395.
86 S. M. Barbon and J. B. Gilroy, *Polym. Chem.*, 2016, **7**, 3589–3598.
87 J. S. Dhindsa, R. R. Maar, S. M. Barbon, M. O. Avilés, Z. K. Powell, F. Lagugné-Labarthet and J. B. Gilroy, *Chem. Commun.*, 2018, **54**, 6899–6902.
88 J. S. Dhindsa, A. Melenbacher, S. M. Barbon, M. J. Stillman and J. B. Gilroy, *Dalton Trans.*, 2020, **49**, DOI: 10.1039/C9DT03417J.
89 M.-C. Chang and E. Otten, *Organometallics*, 2016, **35**, 534–542.
90 R. Mondol, D. A. Snoeken, M.-C. Chang and E. Otten, *Chem. Commun.*, 2017, **53**, 513–516.
91 R. Mondol and E. Otten, *Inorg. Chem.*, 2018, **57**, 9720–9727.
92 A. Van Belois, R. R. Maar, M. S. Workentin and J. B. Gilroy, *Inorg. Chem.*, 2019, **58**, 834–843.
93 C. Goze, G. Ulrich and R. Ziessel, *J. Org. Chem.*, 2007, **72**, 313–322.
94 W. Schorn, D. Grosse-Hagenbrock, B. Oelkers and J. Sundermeyer, *Dalton Trans.*, 2016, **45**, 1201–1207.
95 R. R. Maar, A. Rabiee Kenaree, R. Zhang, Y. Tao, B. D. Katzman, V. N. Staroverov, Z. Ding and J. B. Gilroy, *Inorg. Chem.*, 2017, **56**, 12436–12447.
96 R. Mondol and E. Otten, *Inorg. Chem.*, 2019, **58**, 6344–6355.
97 C. Cui, H. W. Roesky, H.-G. Schmidt, M. Noltemeyer, H. Hao and F. Cimpoesu, *Angew. Chem., Int. Ed.*, 2000, **39**, 4274–4276.
98 R. Mondol and E. Otten, *Dalton Trans.*, 2019, **48**, 13981–13988.
99 R. R. Maar, S. D. Catingan, V. N. Staroverov and J. B. Gilroy, *Angew. Chem., Int. Ed.*, 2018, **57**, 9870–9874.
100 M. Yamamura, M. Albrecht, M. Albrecht, Y. Nishimura, T. Arai and T. Nabeshima, *Inorg. Chem.*, 2014, **53**, 1355–1360.
101 R. G. Hicks and R. Hooper, *Inorg. Chem.*, 1999, **38**, 284–286.
102 R. G. Hicks, L. Öhrström and G. W. Patenaude, *Inorg. Chem.*, 2001, **40**, 1865–1870.
103 T. M. Barclay, R. G. Hicks, A. S. Ichimura and G. W. Patenaude, *Can. J. Chem.*, 2002, **80**, 1501–1506.